

# **An Analysis of Algorithms for In Vivo Fiber Tractography Using DW-MRI Data**

780 Project

Jing Li

Supervised by: Dr. Burkhard Wuensche

The Computer Science Department

The University of Auckland

2005

## **ABSTRACT**

In this paper, several nerve fiber tracking methods which are used to visualize the connectivity of brain regions in vivo are analyzed using noise-affected synthetic diffusion tensor fields with crossing tracts geometry. The simulated DTI dataset is constructed using B-Spline curves wrapped with a tube, which represents a bundle of never fiber tracts. Particularly, we compare three fiber tractography methods, Streamlines, Tensorlines, and Tensor deflection (TEND). The analysis of the simulations revealed that when estimating the crossing trajectories of white matter tracts in human brain, Streamlines simulation completely deviate from the ideal pathway, whereas Tensorlines and TEND methods keep a part of integrated tracts inside the ideal pathway, and are suitable to be used to simulate the tracts of a diffusion tensor field with crossing, branching, merging and brunching tracts geometries.

# Contents

<b>INTRODUCTION</b> .....	<b>1</b>
<b>DIFFUSION TENSOR MAGNETIC RESONANCE IMAGING</b> .....	<b>3</b>
DTI DATA ACQUISITION.....	3
DTI DATA PROCESSING.....	4
LIMITATION OF DIFFUSION TENSOR IMAGING .....	7
<b>FIBER TRACTOGRAPHY MEHTODS</b> .....	<b>8</b>
STREAMLINE TRACKING .....	8
TENSORLINE ALGORITHM .....	10
TENSOR DEFLECTION.....	10
<b>SYNTHETIC TENSOR FIELD</b> .....	<b>12</b>
CONSTRUCTION OF EIGENVALUES AND EIGENVECTORS .....	12
SIMULATION PROCEDURE FOR ADDING NOISE TO A SYNTHETIC TENSOR FIELD .....	13
<b>IMPLEMENTATION</b> .....	<b>16</b>
CONSTRUCTION OF A SYNTHETIC TENSOR FIELD .....	16
GENERATING OF NOISED-CONTAMINATED SYNTHETIC TENSOR FIELDS.....	18
SIMULATIONS OF FIBER TRACKS .....	19
SOFTWARE ARCHITECTURE OF THE APPLICATION .....	21
USER GUIDE .....	22
<b>ERROR MEASUREMENTS</b> .....	<b>24</b>
ERROR MEASUREMENTS OF A SYNTHETIC TENSOR FIELD CONTAINING CROSSING TRACTS.....	24
<i>Error measurements of the average length of the simulated tracts</i> .....	24
<i>Error measurements of the correctness of the simulated tracts</i> .....	26
<i>Least Square Error of the simulated tracts</i> .....	29
ERROR MEASUREMENTS OF A SYNTHETIC TENSOR FIELD CONTAINING MERGING TRACTS.....	31
<i>Error measurements of the average length of the simulated tracts</i> .....	32
<i>Error measurements of the correctness of the simulated tracts</i> .....	34
<i>Least Square Error of the simulated tracts</i> .....	36
<b>CONCLUSIONS</b> .....	<b>38</b>
<b>ACKNOWLEDGEMENTS</b> .....	<b>39</b>
<b>REFERENCES</b> .....	<b>39</b>

## INTRODUCTION

Diffusion tensor image measures diffusion properties of water inside living fibrous tissues such as nerves, muscles, ligaments, tendons, etc. (Basser, Pajevic et al. 2000). The diffusion tensor defines the directions of highest and lowest diffusion and the diffusion coefficients in these directions of water in the living tissues. The directional information of water diffusion in the brain can estimate the structure and the orientation of the never fiber tracts as water tends to diffuse within white matter along the axonal fiber direction in brain (Figure 1).

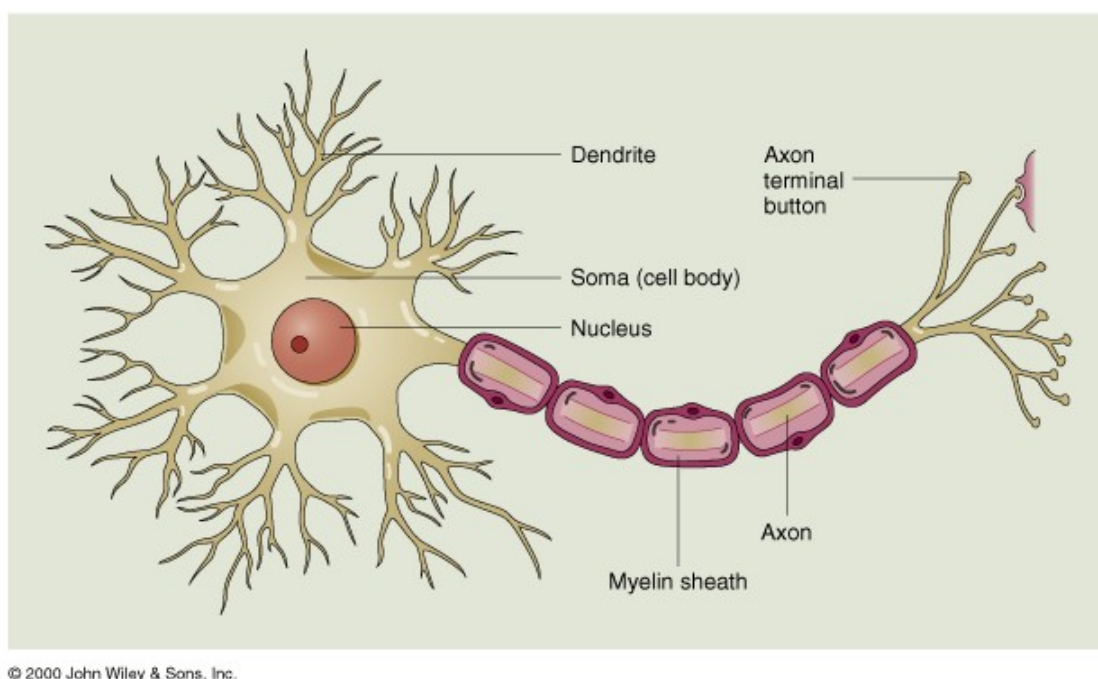


**Figure 1: The basic structure of a nerve cell [1].**

Nerve fiber tractography using DTI is a promising medical research tool for studying and visualizing the nerve fiber tracts in vivo. Streamline algorithm can be used to propagate the nerve fiber trajectories from a vector field which is computed from the diffusion tensor field. It uses only the tensor major diffusion direction to estimate the fiber direction, hence it fails to accurately follow the ideal pathways when it meets the degenerated points as on such points there are no particular diffusion directions. To remedy such fault, the Tensorlines algorithm (Weinstein, Kindlmann et al. 1999) incorporates information about the nearby orientation of the local tensor to propagate stable tracts, and the Tensor Deflection algorithm (TEND)

(Lazar, Weinstein et al. 2003) uses the entire diffusion tensor information to deflect the estimated fiber trajectory.

The three tractography methods, Streamlines, Tensorlines, and Tensor Deflection were implemented in the project. To compare and analyze the three tractography methods, synthetic diffusion tensor fields with crossing tracts are constructed. The tracts simulated by the methods are compared with the ideal pathways of the synthetic tensor fields that are well known in advance. To make the dataset more realistic, Complex Gaussian normal noises with different levels of SNR are added to the real and imaginary channels of the ideal signal for every voxel in the tensor fields (Skare, Li et al. 2000; Jonasson, Hagmann et al. 2003).

## DIFFUSION TENSOR MAGNETIC RESONANCE IMAGING

The Diffusion tensor  $T$  is a symmetric second-order tensor and is presented by a 3x3 symmetric, semi-positive definite matrix only using 6 independent elements

$(D_{xx}, D_{xy}, D_{xz}, D_{yy}, D_{yz}, D_{zz})$ .

$$T = \begin{pmatrix} D_{xx} & D_{xy} & D_{xz} \\ D_{xy} & D_{yy} & D_{yz} \\ D_{xz} & D_{yz} & D_{zz} \end{pmatrix} \quad \text{Equation 1}$$

The six independent elements are determined from a set of diffusion weighted signals. After acquisition of  $T$ , the three principal diffusivities (eigenvalues) known as  $\lambda_1, \lambda_2, \lambda_3$  and diffusion directions (eigenvectors) known as  $e_1, e_2, e_3$  can be calculated from the tensor  $T$  as the eigenvectors and the eigenvalues fulfill the equator Eq. [2] (Young 1993).

$$T \begin{pmatrix} e_1 \\ e_2 \\ e_3 \end{pmatrix} = \begin{pmatrix} \lambda_1 & 0 & 0 \\ 0 & \lambda_2 & 0 \\ 0 & 0 & \lambda_3 \end{pmatrix} \begin{pmatrix} e_1 \\ e_2 \\ e_3 \end{pmatrix} \quad \text{Equation 2}$$

### DTI data acquisition

A diffusion tensor image is estimated from a series of diffusion weighted images that are acquired with applied different diffusion weighted gradient direction vectors. Two commonly used DTI schemes employ 6 or 7 diffusion weighted gradient directions. The relationship of the diffusion weighted (DW) pixel intensity  $S$ , the tensor  $T$  and DW gradient vector is described by the equation Eq. [3] (Papadakis, Xing et al. 1999).

$$S = S_0 \exp(-BG_d^T \bullet T \bullet G_d) \quad \text{Equation 3}$$

where  $S_0$  is the baseline pixel intensity with the DW gradients are set to zero;  $G_d$  is the unit vector describing the DW gradient direction;  $B$  is called the b-factor, which does not rely on DW gradient direction at all.  $S_0$  and  $B$  are usually constants for a tensor field.

We look at the details of the matrix production of  $G_d^T \bullet T \bullet G_d$ .

$$\begin{aligned}
G_d^T \bullet T \bullet G_d &= \begin{pmatrix} G_{dx} & G_{dy} & G_{dz} \end{pmatrix} \bullet \begin{pmatrix} D_{xx} & D_{xy} & D_{xz} \\ D_{xy} & D_{yy} & D_{yz} \\ D_{xz} & D_{yz} & D_{zz} \end{pmatrix} \bullet \begin{pmatrix} G_{dx} \\ G_{dy} \\ G_{dz} \end{pmatrix} \\
&= \begin{pmatrix} G_{dx}D_{xx} + G_{dy}D_{xy} + G_{dz}D_{xz} & G_{dx}D_{xy} + G_{dy}D_{yy} + G_{dz}D_{yz} & G_{dx}D_{xz} + G_{dy}D_{yz} + G_{dz}D_{zz} \end{pmatrix} \bullet \begin{pmatrix} G_{dx} \\ G_{dy} \\ G_{dz} \end{pmatrix} \\
&= G_{dx}^2 D_{xx} + G_{dy}^2 D_{yy} + G_{dz}^2 D_{zz} + 2G_{dx}G_{dy}D_{xy} + 2G_{dx}G_{dz}D_{xz} + 2G_{dy}G_{dz}D_{yz} \\
&= \begin{pmatrix} G_{dx}^2 & G_{dy}^2 & G_{dz}^2 & 2G_{dx}G_{dy} & 2G_{dx}G_{dz} & 2G_{dy}G_{dz} \end{pmatrix} \bullet \begin{pmatrix} D_{xx} \\ D_{yy} \\ D_{zz} \\ D_{xy} \\ D_{xz} \\ D_{yz} \end{pmatrix}
\end{aligned}$$

Defining the six-dimensional (6D) vectors

$$\begin{aligned}
g &= \begin{pmatrix} G_{dx}^2 & G_{dy}^2 & G_{dz}^2 & 2G_{dx}G_{dy} & 2G_{dx}G_{dz} & 2G_{dy}G_{dz} \end{pmatrix}, \\
t &= \begin{pmatrix} D_{xx} & D_{yy} & D_{zz} & D_{xy} & D_{xz} & D_{yz} \end{pmatrix}^T,
\end{aligned}$$

as a result, the Eq.[3] can be rewritten to  $S = S_0 \exp(-Bg \bullet t)$ , then we have

$$g \bullet t = \frac{1}{B} \ln\left(\frac{S_0}{S}\right) \quad \text{Equation 4}$$

Provided the baseline signal  $S_0$ , b-factor  $B$ , the diffusion weighted image pixel intensity  $S$  and the DW gradient direction vectors, then Eq.[4] is a linear function. By solving it, the six unknown elements of the tensor are determined. Actually, the  $g \bullet t$  in the Eq. [4] is called the apparent diffusion coefficients (ADC) (Skare, Li et al. 2000).

### DTI data processing

A general tensor is uniquely defined in terms of its three principal diffusivities (eigenvalues:  $\lambda_1, \lambda_2, \lambda_3$ ) and three corresponding diffusion directions (eigenvectors:  $e_1, e_2, e_3$ ) (Young 1993; Jonasson, Bresson et al. 2005). For a diffusion tensor field,

the tensor at any point is a 3x3 symmetric, semi-positive definite matrix. Its three eigenvalues are all real and the three eigenvectors are mutually orthogonal (Young 1993). The Eq. [5] is used to construct a diffusion tensor field using three real eigenvalues and three orthogonal eigenvectors.

$$T = (e_1 \ e_2 \ e_3) \begin{pmatrix} \lambda_1 & 0 & 0 \\ 0 & \lambda_2 & 0 \\ 0 & 0 & \lambda_3 \end{pmatrix} \begin{pmatrix} e_1 \\ e_2 \\ e_3 \end{pmatrix} \quad \text{Equation 5}$$

where  $\lambda_1 \geq \lambda_2 \geq \lambda_3$ ,  $e_1$  is the major eigenvector associated to the max eigenvalue ( $\lambda_1$ ),  $e_2$  is the medium eigenvector associated to the middle eigenvalue ( $\lambda_2$ ), and  $e_3$  is the minor eigenvector associated to the minimum eigenvalue ( $\lambda_3$ ).

The  $\lambda_1$  and  $e_1$  determine the magnitude and direction of the primary principle axis of the ellipsoid of the tensor. The shapes of the tensor field's ellipsoids are described by the  $\lambda_1 : \lambda_2 : \lambda_3$  ratio. Figure 2 shows the ellipsoids of a tensor field have three types of shapes: highly prolate (e.g.,  $\lambda_1 \gg \lambda_2, \lambda_3$ ) depicted in Figure 2a, oblate (e.g.,  $\lambda_1 \approx \lambda_2 \gg \lambda_3$ ) depicted in Figure 2b, and isotropic (e.g.,  $\lambda_1 \approx \lambda_2 \approx \lambda_3$ ) depicted in Figure 2c.

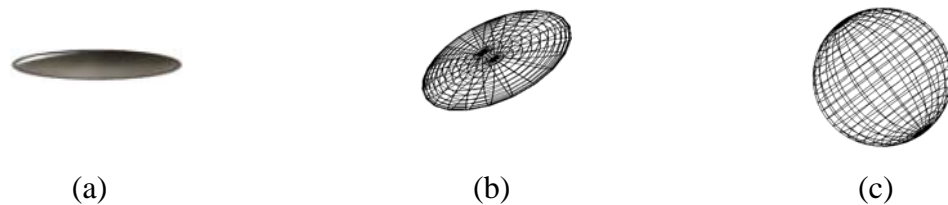


**Figure 2. Tensor shape classification: Linear case (prolate) (a), Planar case (oblate) (b) and Spherical case (isotropic) (c).**

Westin (Westin, Peled et al. 1997) introduced three definitions of linear ( $c_l$ ), planar ( $c_p$ ) and spherical ( $c_s$ ) anisotropy coefficients in 1997:

$$C_l = \frac{\lambda_1 - \lambda_2}{\lambda_1 + \lambda_2 + \lambda_3} \quad \text{Equation 6}$$

$$C_p = \frac{2(\lambda_2 - \lambda_3)}{\lambda_1 + \lambda_2 + \lambda_3} \quad \text{Equation 7}$$



$$C_s = \frac{3\lambda_3}{\lambda_1 + \lambda_2 + \lambda_3} \quad \text{Equation 8}$$

The three coefficients defined by Eq. [6-8] quantify the continuum of classifications within the three cases (linear, planar, and spherical) for real diffusion tensor data.

If a tensor has a planar shape ellipsoid (planar anisotropy) depicted in Figure 2b or a spherical shape ellipsoid (isotropy) depicted in Fig. 2c at a point P, the point P is a degenerate point (Hesslink, Levy et al. 1997), at which the fiber tracts may cross, merge, branch. The two eigenvectors with nearly equivalent eigenvalues have not particular orientations, and span a particular plane in the case of planar anisotropy, and water diffuses uniformly in the plane. For isotropy region, none of three eigenvectors are individual meaningful, they have not particular orientations and span a sphere, and water is distributed uniformly in any direction. The noise in the MRI data may make a point as degenerate point which should not be.

The diffusion tensor has two important measurements: mean diffusivity and anisotropy. The mean diffusivity is defined as the average of the three eigenvalues of the tensor as Eq. [9]. The anisotropy is defined as Eq. [10] (Wuensche and Lobb 2003).

$$\lambda_{mean} = \frac{\lambda_1 + \lambda_2 + \lambda_3}{3} \quad \text{Equation 9}$$

$$\lambda_{anisotropy} = \text{trace}((T - \lambda_{mean}I)^2) / \lambda_{mean}^2 \quad \text{Equation 10}$$

where the  $I$  is an identity 3x3 matrix.

The mean and the anisotropy are used to identify the regions of grey matter, white matter and cerebrospinal fluid(CSF) (Pierpaoli, Jezzard et al. 1996; Wuensche and Lobb 2003) in human brain. White matter region has the properties of

$\lambda_{anisotropy} \geq 0.25$  and  $5 * 10^{-6} < \lambda_{mean} < 10^{-3}$ , while CSF region with  $\lambda_{mean} \geq 10^{-3}$ , grey matter region with  $\lambda_{anisotropy} < 0.25$  and  $5 * 10^{-6} < \lambda_{mean} < 10^{-3}$ .

## **Limitation of Diffusion tensor imaging**

When studying the axonal architecture using DTI data, we should understand there are some limitations with the data due to the conventional DTI data acquisition and processing techniques. Mori(Mori and Zijl 2002) pointed out three main limitations: a voxel containing more than one fiber tracts with different orientations may not be handled properly; DTI can not provide information on cellular-level fiber connectivity, which multiple fiber tracts from individual cells may merge into or branch out from one voxel; Afferent pathways of axonal tracts which carry information from the sense organs towards the CNS and efferent pathways of axonal tracts which carry signals from the CNS towards the target organs (Shahar), can not be verified from the direction of water diffusion. Moreover, the noises generated during the DTI acquisition processing due to several reasons such as the air, patient's motion, can affect the accuracy of the measured DT data, and may destroy the property that it is semi-positive definite.

## FIBER TRACTOGRAPHY MEHTODS

There are mainly two classification of the nerve fiber tracking methods, physics-based and statistical methods. Streamlines, Tensorlines and Tensor deflection which are based on the diffusion direction information of the tensor field when propagating the tracts belong to neither category. They are simply based on the diffusion information at a point and they are no real underlying physical or statistical methods. To simulate the nerve fiber tracks using the three methods, first find the initial locations (seed points) in the region of interests which are determined by the mean diffusivity and the diffusion anisotropy, then from the starting point, bidirectional tracks determined by the diffusion tensor  $T$  at the current position are been propagated as the eigenvector calculated from the local tensor is without sign. The integration is along with a certain direction which is calculated differently for Streamline, tensor Line, and tensor deflection methods. For example, the propagating of streamline method just follows the principal diffusion direction ( $e_1$ ). The tracks were terminated where they reach the volume boundary of the tensor field or they enter into the regions of non-interest, such as the regions of grey matter and CND in human brain.

### Streamline tracking

Streamlines tracking is used on vector fields. It visualizes the structure of the vector field. When it is employed to diffusion tensor fields, it integrates the fiber tracts only based on the major diffusion direction ( $e_1$ ) of the local tensor. It is defined as the solution to the differential equation

$$\frac{S(t)}{dt} = v(S(t)) \quad \text{Equation 11}$$

where the  $v(S(t))$  is the unit tangent vector at  $S(t)$ ,  $t$  is the time step. The fiber trajectories of the vector field can be generated by integrating Eq. [11] with an initial condition  $S(0) = S_0$  which specifies a starting point of the fiber tract trajectory. The Taylor series expansion can be used to derive a solution method. There are three most common solvers, Euler, second-order Mid-point and fourth-order Runge-Kutta (RK4) which take one, two and four terms of the expansion of the Taylor series respectively.

The higher order the solver is, the bigger time step it can use, but more derivation computation on each step it costs. Hence, RK4 is computational more expensive than Mid-point (Basser, Pajevic et al. 2000; Wuensche 2004). The streamline integration using a first order Euler method is depicted in Figure 3.

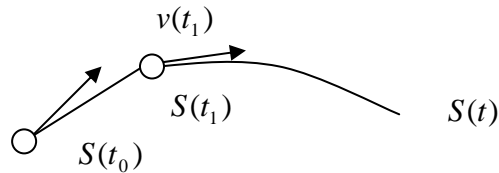


**Figure 3: Streamline integration using a first order Euler method.**

The degenerate points of the tensor fields described in section “DTI processing” need to be checked when simulating the fiber tract trajectories due to lack of particular meaningful diffusion direction on such points and the diffusion direction spins on a plane or a sphere (Hesslink, Levy et al. 1997). The streamline integration should be terminated at singularity points as the fast diffusion direction is arbitrary which will mislead the streamline propagation. Figure 4 shows such example. The degenerate point is checked only as  $\lambda_1 \approx \lambda_2$  rather than at least two eigenvalues equal (e.g.  $\lambda_1 \approx \lambda_2$ , or  $\lambda_1 \approx \lambda_3$ , or  $\lambda_2 \approx \lambda_3$ ) as the major eigenvector corresponding to the  $\lambda_1$  still is meaningful on the case of  $\lambda_2 \approx \lambda_3$ .

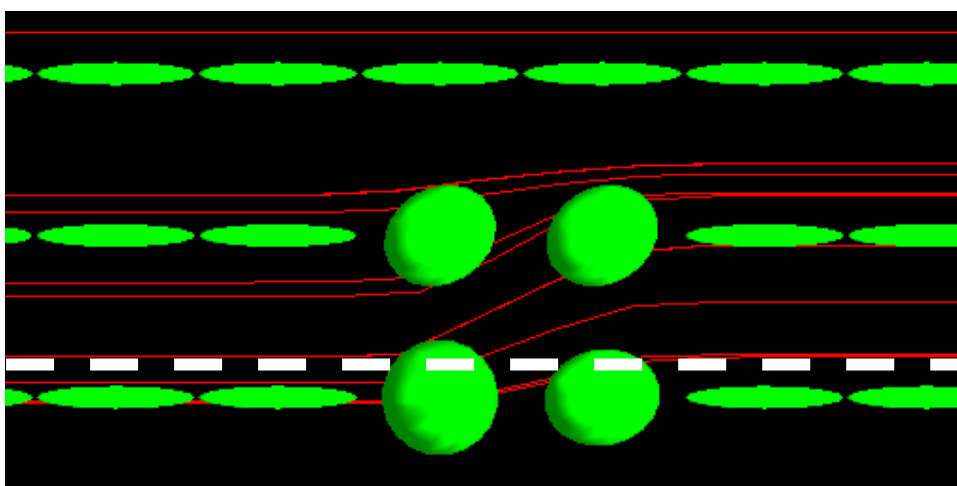


**Figure 4: The ideal fiber tracts path denoted by the dotted white line and the visualization of streamline in red through anisotropy (left and right) and isotropic (middle) regions in synthetic tensor field.**

## Tensorline algorithm

Weinstein(Weinstein, Kindlmann et al. 1999) introduced Tensorline fiber tracking method in 1999. Their technique not only counts on the principal diffusion direction of the local tensor, but also the nearby orientation information of the local tensor by adding an advection term in a standard diffusion-based propagation method. Hence, the propagation direction is a combination of the principal diffusion direction ( $e_1$ ), the incoming vector from the previous integration step ( $v_{in}$ ) and the outgoing vector which is the incoming vector transformed by the tensor matrix ( $v_{out}$ ).

When doing propagation of fiber tracts, first an outgoing direction vector  $v_{out}$  is computed using the incoming direction  $v_{in}$  and the tensor (Eq. [12]). The  $v_{in}$  is the direction of the previous propagation step, and the  $v_{out}$  is the incoming vector transformed by the tensor matrix.

$$v_{out} = Tv_{in} \quad \text{Equation 12}$$

The principal diffusion direction ( $e_1$ ),  $v_{in}$  and  $v_{out}$  are combined using Eq. [13] to gain the proper propagation direction  $v_{prop}$  for current step.

$$v_{prop} = c_l e_1 + (1 - c_l)((1 - w_{punct})v_{in} + w_{punct}v_{out}) \quad \text{Equation 13}$$

where,  $c_l$  is the linear anisotropy coefficient of the local tensor computed using Eq. [6];  $w_{punct}$  is a weighting factor controlled by users, which varies from 0 to 1. The weighting factor affects how much the propagation should be encouraged to “puncture” to the incoming path when it goes through planar tensors by changing the weights on the incoming vector and the outgoing vector (Weinstein, Kindlmann et al. 1999). Weinstein claimed that when integrating the fiber tracts in human brain, the  $w_{punct}$  of 0.20 worked well in practice.

## Tensor deflection

Lazar(Lazar, Weinstein et al. 2003) introduced Tensor Deflection fiber tracking method in 2003, which was called TEND. The method uses the entire diffusion tensor information to deflect the incoming vector ( $v_{in}$ ) direction which is got from the previous integration step.

$$v_{out} = Tv_{in} \quad \text{Equation 14}$$

where  $v_{out}$  is the incoming vector transformed by the tensor matrix.

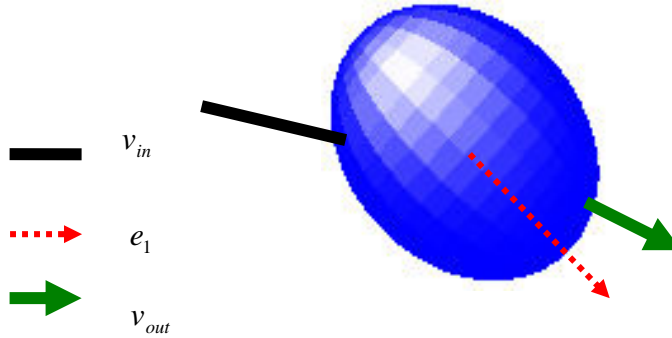


**Figure 5: Illustration of tensor deflection for a diffusion tensor**

In the TEND algorithm, the incoming vector can be described using a linear combination of the eigenvectors of the tensor.

$$v_{in} = \alpha_1 e_1 + \alpha_2 e_2 + \alpha_3 e_3 \quad \text{Equation 15}$$

where  $\alpha_1, \alpha_2, \alpha_3$  are the projections of incoming vector onto the axes of the coordinate system given by  $e_1, e_2, e_3$ .

$$\begin{aligned} \alpha_1 &= v_{in} \cdot e_1 \\ \alpha_2 &= v_{in} \cdot e_2 \\ \alpha_3 &= v_{in} \cdot e_3 \end{aligned} \quad \text{Equation 16}$$

The incoming vector is deflected toward the predominant principal eigenvector for a tensor is more anisotropic. The less anisotropic the tensor is, the less amount the incoming vector is deflected by the tensor.

For the formula of the Tensorlines algorithm (Eq. [13]), if  $c_l$  equals 1, the Tensorlines algorithm is equivalent to Streamlines method; if  $c_l$  equals 0 and the puncture coefficient  $w_{punct}$  is set to 1, the tensorlines algorithm is equivalent to Tensor deflection method. We can see that the Tensorlines algorithm is the combination of the Streamlines and the Tensor deflection methods.

## Synthetic Tensor Field

In order to quantitatively compare the fiber tracts trajectory algorithms Synthetic tensor fields (Westin, Maier et al. 1999; Basser, Pajevic et al. 2000; Jonasson, Hagmann et al. 2003; Lazar and Alexander 2003; Lazar, Weinstein et al. 2003) are required. A synthetic tensor field is reconstructed using Eq. [5] in terms of three eigenvalues and eigenvectors. To make the synthetic tensor more realistic, Rician noise should be added to the tensor field. But when the SNR of the DTI imaging is above 3, we can approximate this noise with Gaussian normal noise.

### Construction of Eigenvalues and Eigenvectors

The three eigenvalues and three eigenvectors need to be determined before applying Eq. [5] to construct the synthetic tensor fields. Different types of fibers have eigenvalues in certain range (Papadakis, Xing et al. 1999).

The three eigenvectors are determined by piecewise functions. In isotropic region, they can set to uniformly distributed unit vectors which are mutually orthogonal. In anisotropic region, the tangent unit vector of the ideal pathways of the synthetic fiber tracts in the synthetic tensor fields is set to  $e_1$ . Because a Frenet-frame of a space curve is made of three vectors: tangent, normal, binormal vectors which are mutually orthogonal, the Frenet-frame can be used to define the values for  $e_1$ ,  $e_2$  and  $e_3$ . Its tangent vector indicates the direction of the pathway and is assigned to  $e_1$ . Its normal and binormal vectors are assigned to  $e_2$  and  $e_3$  respectively. The synthetic fiber tracts should be smooth and low curvature to correspond with the natural properties of the real never fiber tracts.

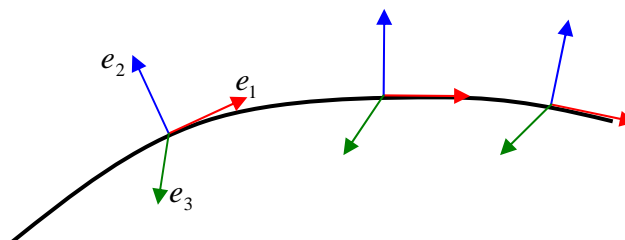


**Figure 6: Using the Frenet-frame of a space curve to determine the eigenvectors of tensors of a synthetic tensor field.**

## Simulation procedure for adding noise to a synthetic tensor field

To make the synthetic diffusion tensor data more realistic, complex Gaussian normal noise with zero mean and the standard deviation corresponding to the desired SNR should be added to the real and imaginary channels of the ideal signal for every voxel in the data. The procedure of adding noise to a synthetic tensor field is the reverse of the process for DTI data acquisition, which solves the linear Eq. [4] to get the six independent elements of a diffusion tensor from the baseline signal  $S_0$ , b-factor  $B$ , the diffusion weighted image pixel intensity  $S$  and the DW gradient direction vectors. Now, we have the noise-free tensor matrix, from that the ideal signal can be computed. After knowing the ideal signal, we need to compute the noised tensor with desired SNR level by assuming the baseline signal  $S_0$ , b-factor  $B$ , and the DW gradient direction vectors. The detail procedure is depicted in 7 steps (Skare, Li et al. 2000).

- 1) Compute the noise-free tensor using Eq. [5] in terms of user-defined three mutually orthogonal eigenvectors and three corresponding eigenvalues, and get the six independent elements ( $D_{xx}, D_{yy}, D_{zz}, D_{xy}, D_{xz}, D_{yz}$ ) from the tensor.
- 2) Define the six diffusion weighting gradient direction vectors  $q_i$ , as

$$\begin{aligned}
 q_1 &= \frac{1}{\sqrt{3}} \begin{bmatrix} 1 \\ 1 \\ 1 \end{bmatrix}, q_2 = \frac{1}{\sqrt{3}} \begin{bmatrix} -1 \\ -1 \\ 1 \end{bmatrix}, q_3 = \frac{1}{\sqrt{3}} \begin{bmatrix} 1 \\ -1 \\ -1 \end{bmatrix}, \\
 q_4 &= \frac{1}{\sqrt{3}} \begin{bmatrix} -1 \\ 1 \\ -1 \end{bmatrix}, q_5 = \frac{1}{\sqrt{2}} \begin{bmatrix} 1 \\ 1 \\ 0 \end{bmatrix}, q_6 = \frac{1}{\sqrt{2}} \begin{bmatrix} 1 \\ 0 \\ 1 \end{bmatrix}
 \end{aligned}
 \tag{Equation 17}$$

The six apparent diffusion coefficients (ADC) without noises corresponding to the  $q_i$  can be computed from the tensor  $T$  and the six diffusion weighting gradient direction vectors  $q_i$  using Eq. [18].

$$ADC_i = q_i^T T q_i
 \tag{Equation 18}$$

By replacing the  $q_i$  in Eq. [18] with the vectors defined in Eq. [17], we can get a transformation matrix for transforming the six independent elements of tensor  $T$  to six ADC.



$$\begin{pmatrix} ADC_1 \\ ADC_2 \\ ADC_3 \\ ADC_4 \\ ADC_5 \\ ADC_6 \end{pmatrix} = A \begin{pmatrix} D_{xx} \\ D_{yy} \\ D_{zz} \\ D_{xy} \\ D_{xz} \\ D_{yz} \end{pmatrix} \quad \text{Equation 19}$$

$$\text{where } A = \frac{1}{3} \begin{pmatrix} 1 & 1 & 1 & 2 & 2 & 2 \\ 1 & 1 & 1 & 2 & -2 & -2 \\ 1 & 1 & 1 & -2 & -2 & 2 \\ 1 & 1 & 1 & -2 & 2 & -2 \\ \frac{3}{2} & \frac{3}{2} & 0 & 1 & 0 & 0 \\ \frac{3}{2} & 0 & \frac{3}{2} & 0 & 1 & 0 \end{pmatrix} \quad \text{Equation 20}$$

- 3) Once the ADC is determined using Eq.[18] by step 2, the “ideal” noise-free DW signal  $S_i, i = 1..6$  are calculated from Eq.[3], assuming a constant ideal value of the baseline signal  $S_0 = 1000$  , and a constant value of the B-factor  $b = 1000 \text{ s/mm}^2$  for each fiber type and DTI scheme. The choice of  $S_0$  is very arbitrary, but the ratio of  $S_0$  to the standard deviation of the noise is very important. The ration is called signal-to-noise ratio (SNR). As long as the noise is scaled according to the ratio,  $S_0$  can be set to one.

$$SNR = S_0 / SD \quad \text{Equation 21}$$

where  $SD$  is the standard deviation of normal Gaussian noise. For a standard DTI the currently accepted value for the B-factor is around  $1000 - 1500 \text{ s/mm}^2$  , however some people believe that high values for the B-factor of around  $3000 - 4000 \text{ s/mm}^2$  are needed to help to resolve more complex fiber connectivity, such as crossing fiber tracts (Tuch 2004).

- 4) To get complex noise-contaminated signals, the noise-free signal  $S_i, i = 1..6$  computed in previous step is treated as a complex number  $Z = a + ib$  , where  $Mod(Z) = S = \text{sqrt}(a^2 + b^2)$  . For simplicity, we set  $a = S, b = 0$  , and independent normal Gaussian noises are then superimposed upon to the complex number’s real and imaginary parts separately, which is demonstrated in Eq. [22].

$$Z' = (S_i + noiseA) + i * (noiseB), i = 1..6 \quad \text{Equation 22}$$

where *noiseA* and *noiseB* are independent random samples from a Gaussian distribution of mean zero and standard deviation SD. The SD is defined by the desired SNR in Eq. [21] which can be set to any desired level depending on the simulations requirements. It is not hard to get a Gaussian random sample with a desired mean and variance. First the unit normal random variables with *mean* = 0 and *variance* = 1 are computed using *gasdev* (Press, Flannery et al. 1992), then the noise is modified using Eq.[23].

$$noise = mean + SD * unit\_noise \quad \text{Equation 23}$$

The noise-contaminated signal is computed as the magnitude of the complex number.

$$noiseS_i = \text{mod}(Z') = \text{sqrt}((S_i + noiseA)^2 + (noiseB)^2) \quad \text{Equation 24}$$

- 5) From the step 4, the noise-contaminated signals are obtained, then the noise-contaminated ADC can be calculated using Eq. [4] (note: the  $g \bullet t$  in the Eq. [4] is the ADC).
- 6) The relationship of the ADC and the elements of a tensor are showed in Eq. [19] and Eq. [20]. The six noised affected independent elements of a tensor can be obtained by reversing step 2. The inverse matrix of A is showed in Eq. [25].

$$A^{-1} = \begin{pmatrix} -5/4 & -3/4 & -1/4 & -3/4 & 2 & 2 \\ 1 & 1/2 & 1/2 & 1 & 0 & -2 \\ 1 & 1 & 1/2 & 1/2 & -2 & 0 \\ 3/8 & 3/8 & -3/8 & -3/8 & 0 & 0 \\ 3/8 & -3/8 & -3/8 & 3/8 & 0 & 0 \\ 3/8 & -3/8 & 3/8 & -3/8 & 0 & 0 \end{pmatrix} \quad \text{Equation 25}$$

- 7) The six noise-affected elements are used to construct the noised-synthetic diffusion tensor using Eq. [1] as the diffusion tensor is symmetric.

Using this method to superimpose noise to the DT data guarantees the final noise-contaminated DT is a 3x3 symmetry, semi-positive definite matrix.

## IMPLEMENTATION

The Streamlines, Tensorlines and TEND methods are tested using a synthetic tensor field with crossing fiber tracts with different levels of SNR. We first create a synthetic tensor field with crossing fiber tracts, superimpose uniformly distributed Gaussian noise with different levels of SNR to the tensor and integrate the fiber pathways using Streamlines, Tensorlines and TEND techniques.

### Construction of a Synthetic Tensor Field

The synthetic tensor fields we construct have  $32 \times 32 \times 3$  sample points. A B-Spline space curve wrapped with a tube is used to present a synthetic fiber tract. The basic idea is that tensors inside the tube are anisotropic; their eigenvectors are defined by the Frenet-frame of the B-Spline space curve. On the other hand, the tensors outside the tube are isotropic; their eigenvectors are random mutually orthogonal vectors. The diffusion values of the isotropic tensor and anisotropic tensor are the following:

$$T_{isotropy}(\lambda_1 \quad \lambda_2 \quad \lambda_3) = (3 * 10^{-4} \quad 3 * 10^{-4} \quad 3 * 10^{-4})$$
$$T_{anisotropy}(\lambda_1 \quad \lambda_2 \quad \lambda_3) = (7 * 10^{-4} \quad 2.5 * 10^{-4} \quad 0.4 * 10^{-4})$$

The value's units are  $mm^2/s$  (Lazar, Weinstein et al. 2003).

The Frenet-frame of a B-Spline curve is made of the tangent, normal and binormal vectors. The tangent vector is computed by differentiating the parametric function of the B-Spline curve. The normal vector is the cross production of the tangent vector and the acceleration vector that is assumed normally to be a unit vector (0, 1, 0). If the assumed acceleration vector is collinear to the tangent vector, it is reset to a unit vector (1, 0, 0). The binormal vector is computed by taking the cross production of the tangent and normal vectors after obtaining the tangent and normal vectors.

Each tensor in a 3D volume is tested if it is in the tube of the B-Spline by finding the closet point on the B-Spline curve and computing the distance between the tensor and the closet point. In this application the closet point is found using binary searching the B-Spline curve which won't cause ambiguity case as the B-Spline is constructed to be smooth and low curvature (Figure 7).

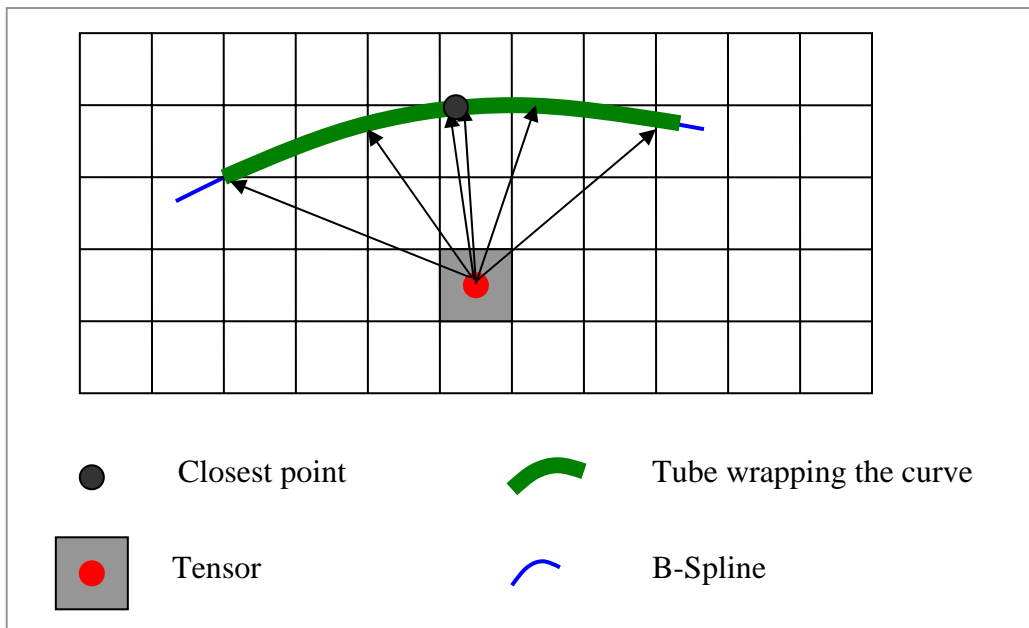


Figure 7: Finding closest point on the B-Spline curve using binary searching.

The synthetic tensor imaging with crossing fiber tracts is constructed by combining two synthetic tensor fields with single fiber tracts in a way of averaging their tensors in a region containing the crossing tracts. Figure 8 shows the crossing B-Spline tubes and the synthetic tensor field constructed by the B-Spline tubes. It is noticed that the tensors in the region containing crossing tracts are isotropic.

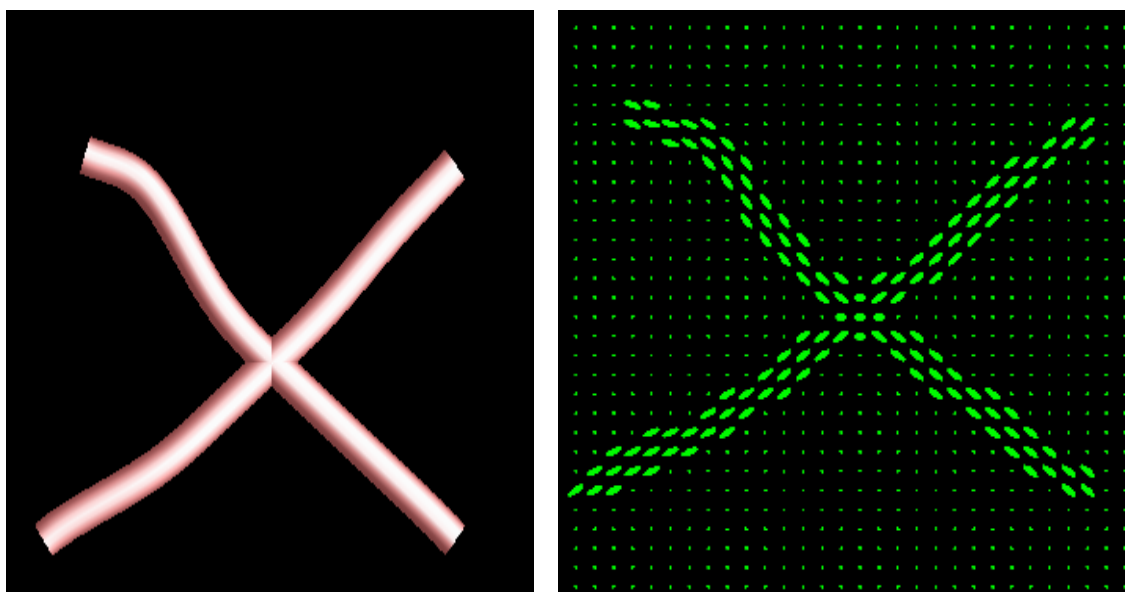
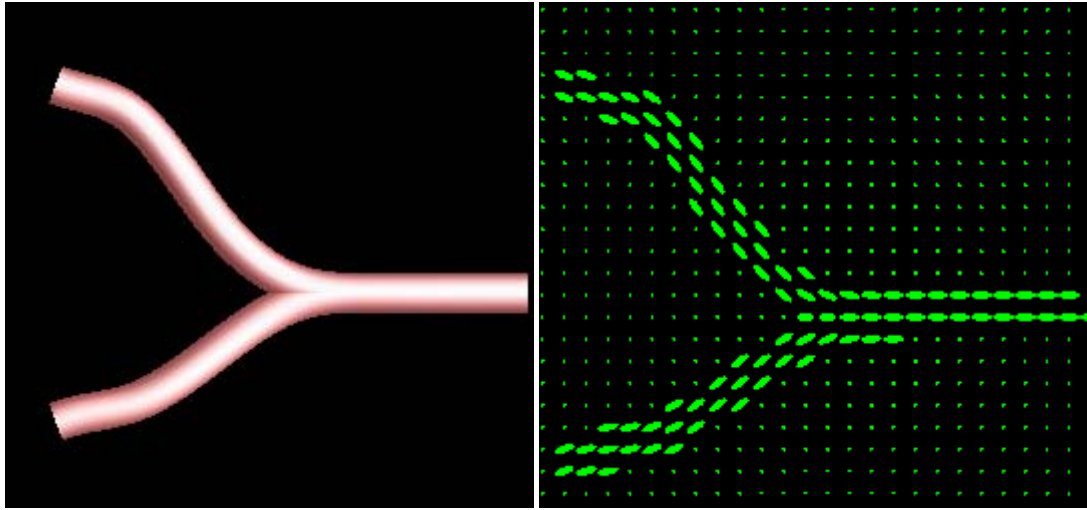


Figure 8: Right image shows the synthetic tensor fields constructed by the crossing tracts which are presented using two pink B-Spline tubes displayed in left image.

In the application, we also constructed a synthetic tensor field in which the fiber tracts merge together (shown in Figure 9). For this tensor field, the tensors in the region containing the merging tracts are anisotropic.



**Figure 9:** Right image shows the synthetic tensor fields with merging tracts which are presented using two pink B-Spline tubes displayed in left image.

To make the synthetic tensor field more realistic, Rician noise should be added to it (Henkelman 1985; Gubjartsson and Patz 1995). In this application, Gaussian normal noises are added to the tensor rather than Rician noise as the SNR level of the noises are assumed greater than 3 (Jonasson, Hagmann et al. 2003).

### **Generating of noised-contaminated synthetic tensor fields**

The procedure of adding Gaussian normal noises to the synthetic tensor field is strictly followed the seven steps depicted in the previous section of “Simulation procedure of adding noise to synthetic tensor field”. The noises with SNR of level 8, 16, 32, 64 ...100000 are superimposed to the tensor field to test the fiber tracking algorithms. Figure 10 shows the results of adding Gaussian normal noises with different levels of SNR to the synthetic tensor field containing crossing fiber tracts.

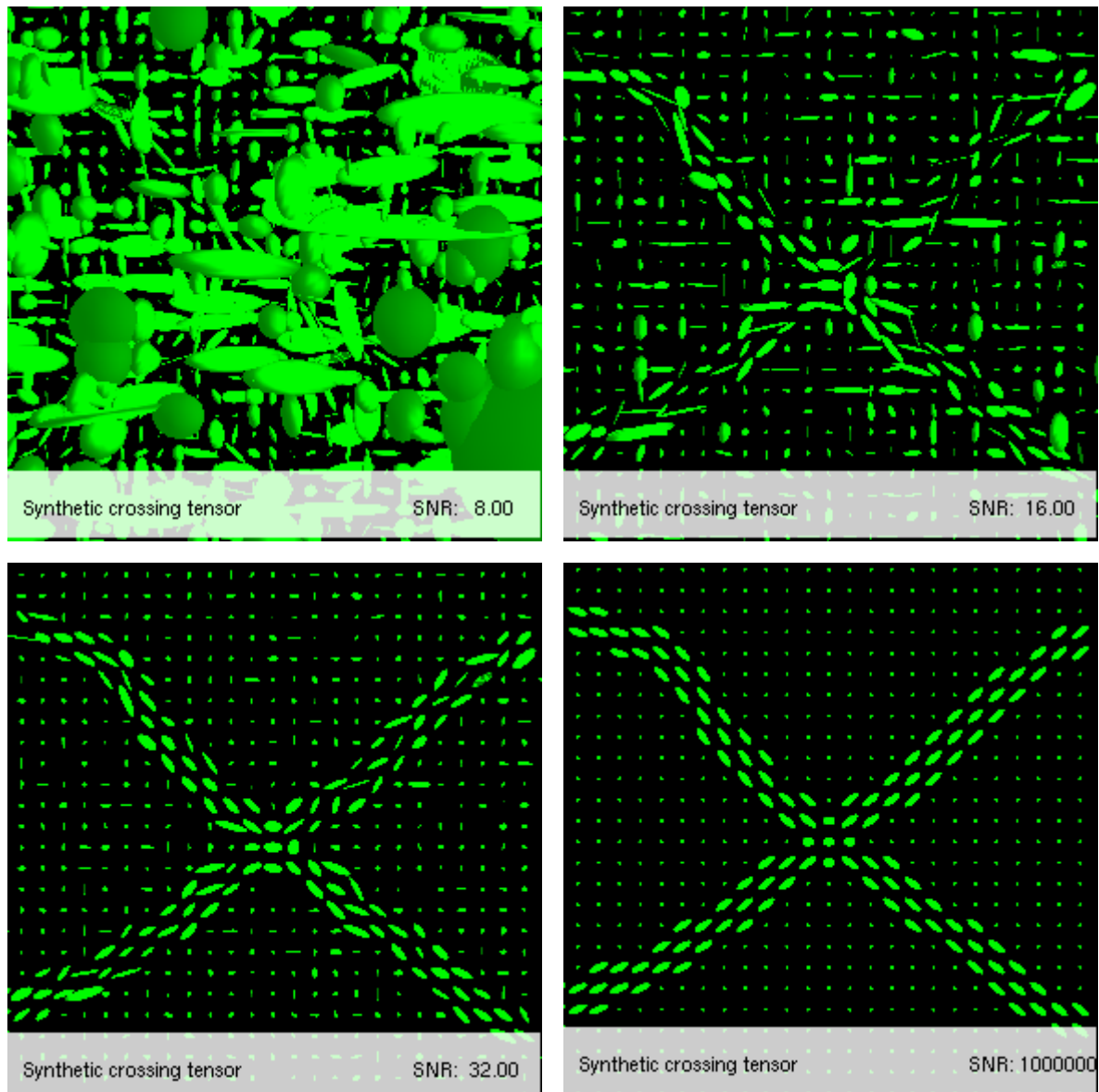


**Figure 10: Noised-contaminated synthetic tensor fields with the geometry of crossing fiber tracts with different level of SNR.**

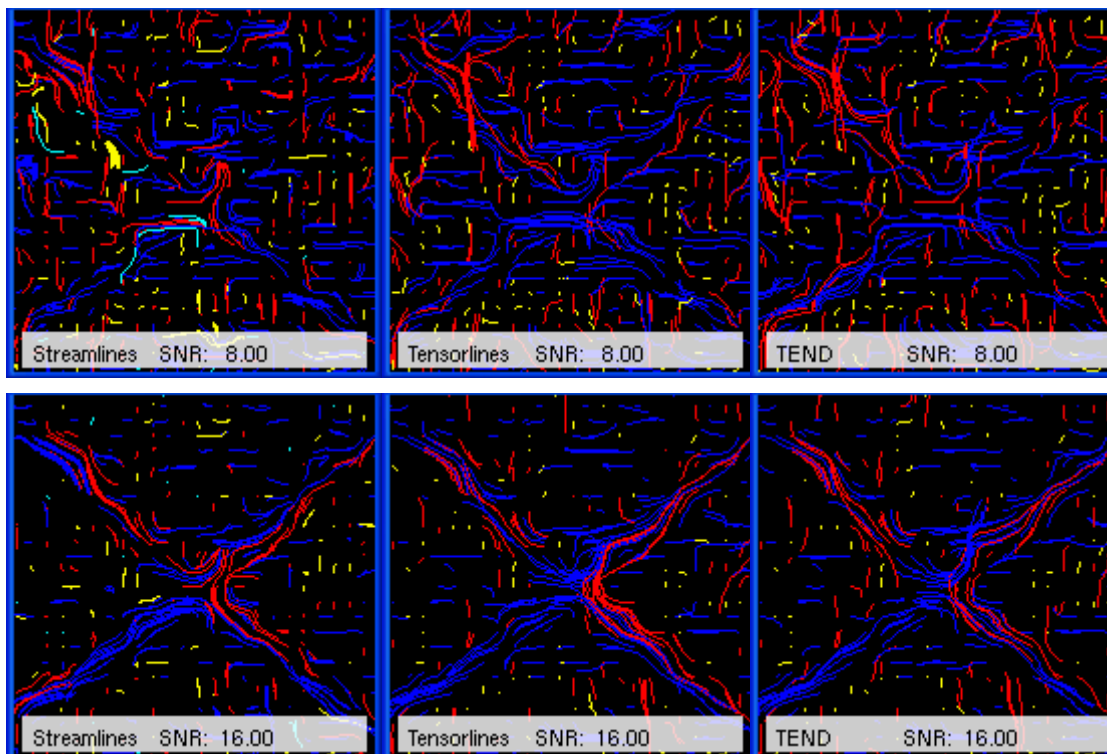
### **Simulations of fiber tracks**

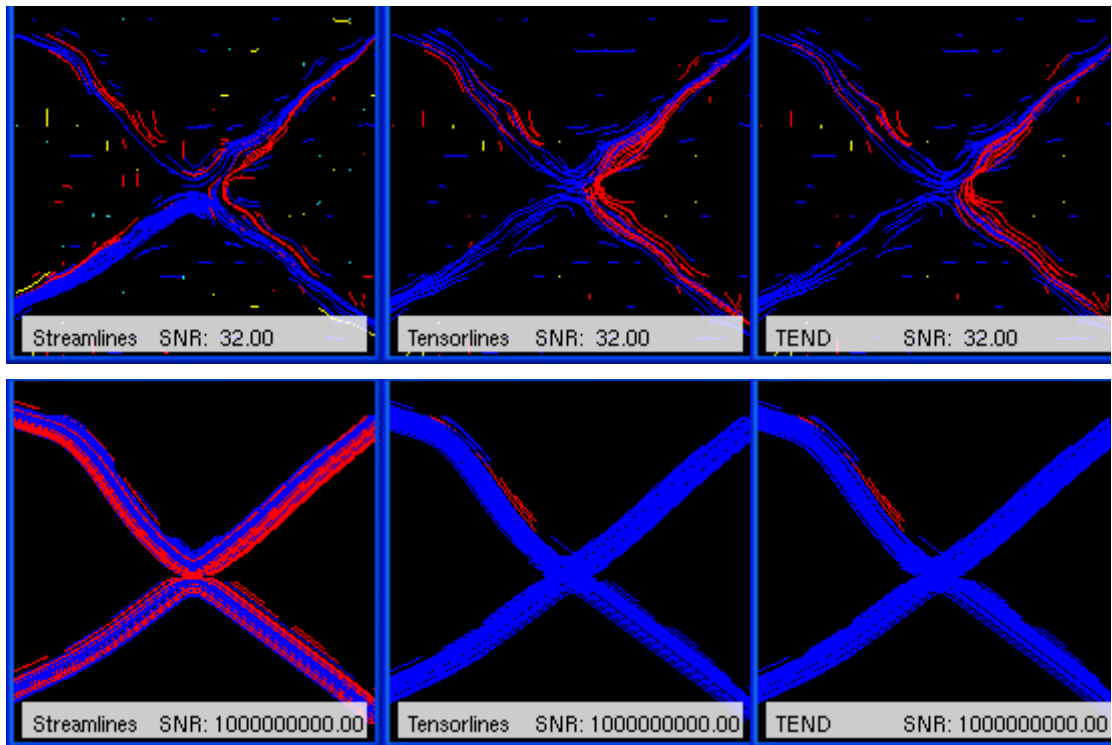
Streamlines, Tensorlines and Tensor Deflection (TEND) with Mid-point and RK-4 integration methods are implemented and tested on the noised-affected synthetic tensor fields with crossing fiber tracts with different levels of SNR. The simulations start with choosing seed points for propagating observed fiber tracts. For each fiber tractography method, each tensor is test if it meets the seed point's criteria. For instant, if the tensor's anisotropy is greater than 0.6 in the application, then it is a seed point.

After determining the seed point, two simulated tracts are issued from the seed point's center with a little offsets on XYZ directions. The two tracts extend along with the positive  $e_1$  direction and negative  $e_1$  direction as  $e_1$  is not able to verify if the pathway is afferent or efferent. The simulation is terminated when the integration of fiber tracts into a region where the tensors' anisotropy is less than 0.2.

On each step of computing the outgoing vectors of the local tensors from the incoming vectors obtained from previous simulation step, the  $e_1$  of the local tensors are test first with the incoming vectors to see if the angle between them is less than great than 90 degree. If the angle is, then the  $e_1$  should be flipped, hence the outgoing vectors are calculated based on the flipped  $e_1$ .

The main goal of the simulations is to test which fiber tracking algorithm is reliable and stable on the regions containing fiber tracts with complex geometries, such as crossing, merging, branching. Figure 11 shows the simulation results. The integrated pathways of the fiber tracts in the synthetic tensor fields are colored in different colors which show the pathways' orientation in 3D (actually in 2D as the simulation results are only displayed on a XY plane). The pathways extending mainly on X, Y, Z directions are colored in blue, red and magenta respectively, other pathways are colored in yellow.





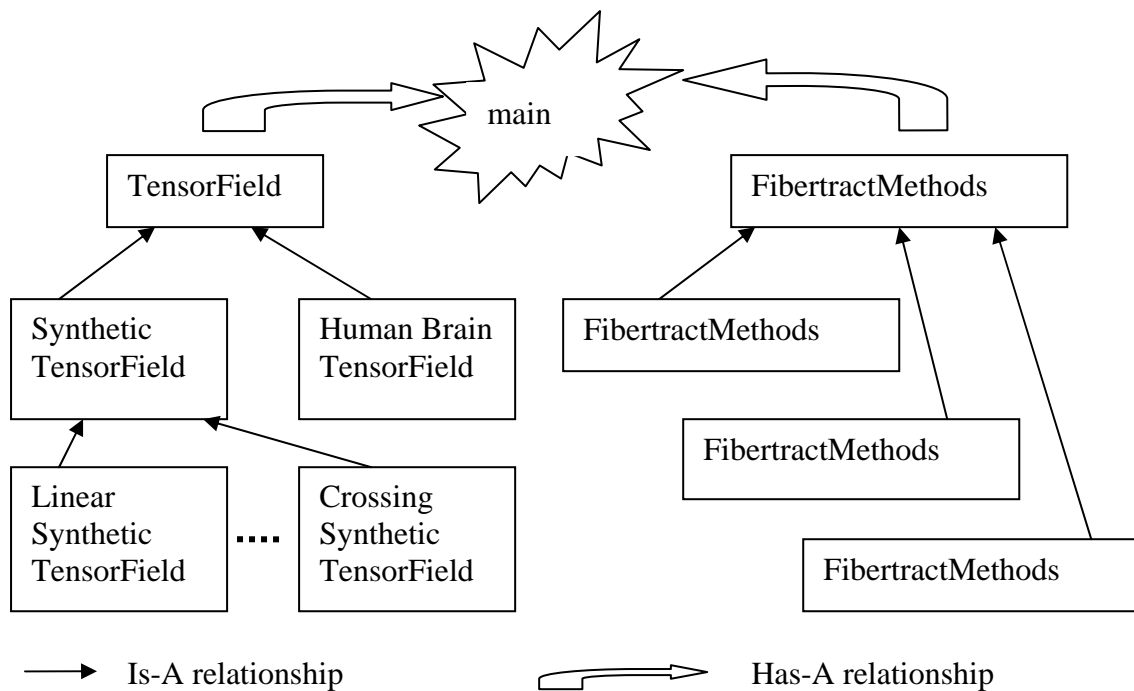
**Figure 11: Simulations of fiber tracts propagation using Streamline, Tensorline, TEND on noised-affected synthetic tensor fields containing crossing tracts with different levels of SNR.**

Figure 11 indicates that Tensorlines and TEND perform similarly for the simulated tensor field.

### **Software architecture of the application**

The application is implemented in C++, using the OpenGL, GLU and GLUT libraries. There are two main classes: TensorField class and FibertractMethods class. The mainloop is developed using the GLUT API rather than Windows 32 API in order to make the application Operating System platform independent. It is very easy to add new subclass for new types of synthetic tensor fields to the TensorField class without changing any structure of the software. Similarly it is very easy to implement new fiber tracts algorithms and test them on existing tensor field without any changing to the structure of the software. Figure 12 demonstrates the software design of our framework for the fiber tracking simulations.





**Figure 12: Software architecture of the platform for the fiber tracts simulations.**

## User Guide

In the application, the mouse movements are used to rotate the rendered tensor fields and the simulated fiber tracts around the center of the 3D space in a similar way of rotating a 3D object in both hands. The following keys can be used to change application settings:.

Key s/S: switch the rendering among

- Tensor field showed in ellipsoids with pathways simulated using Streamline
- Colored pathways simulated using Streamline
- Tensor field showed in ellipsoids with pathways simulated using Tensorline
- Colored pathways simulated using Tensorline
- Tensor field showed in ellipsoids with pathways simulated using TEND
- Colored pathways simulated using TEND

- Ideal pathways of the synthetic tensor field showed tubes constructed by B-Spline space curves.

Key w/W: increase/decrease the user-controlled parameter  $w_{punct}$  for Tensorline simulations. The parameter  $w_{punct}$  varies from 0 to 1.

## Error Measurements

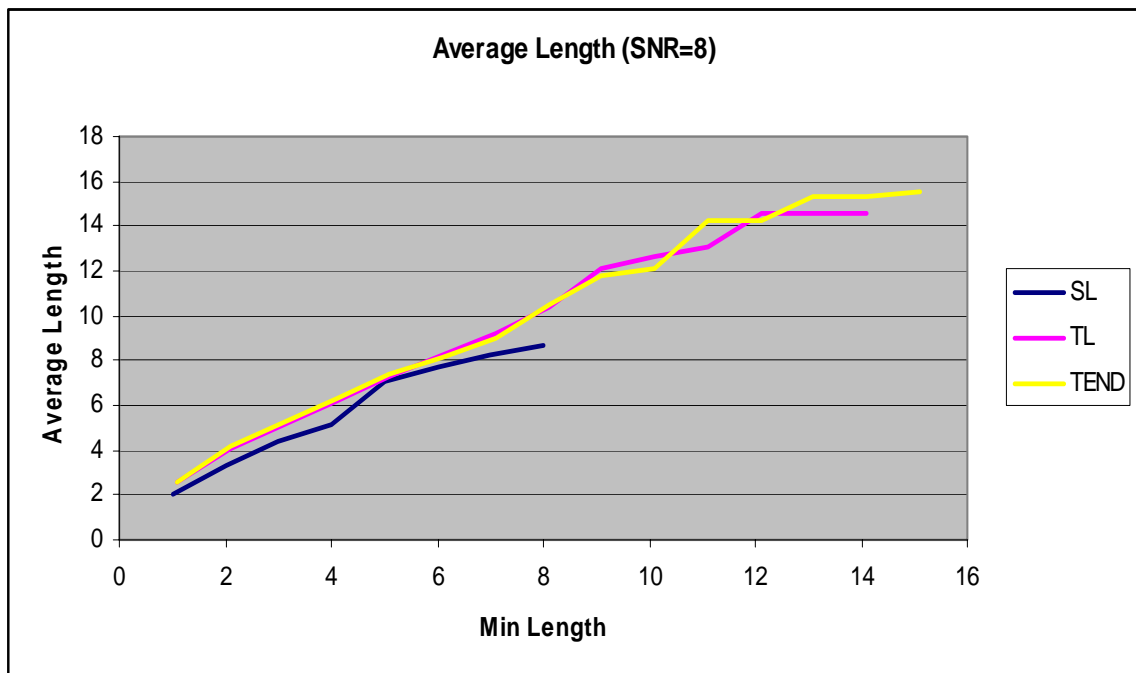
The error of the three tract methods, Streamlines, Tensorlines, Tensor Deflection (TEND) can be measured in three ways: 1. The average length of the simulated tracts; 2. The number of the tracts which follow the ideal tracts correctly; 3. The least square error (LSE) of the simulated tracts. In the follow sections, SL stands for Streamline, TL for Tensorlines in the charts and the tables.

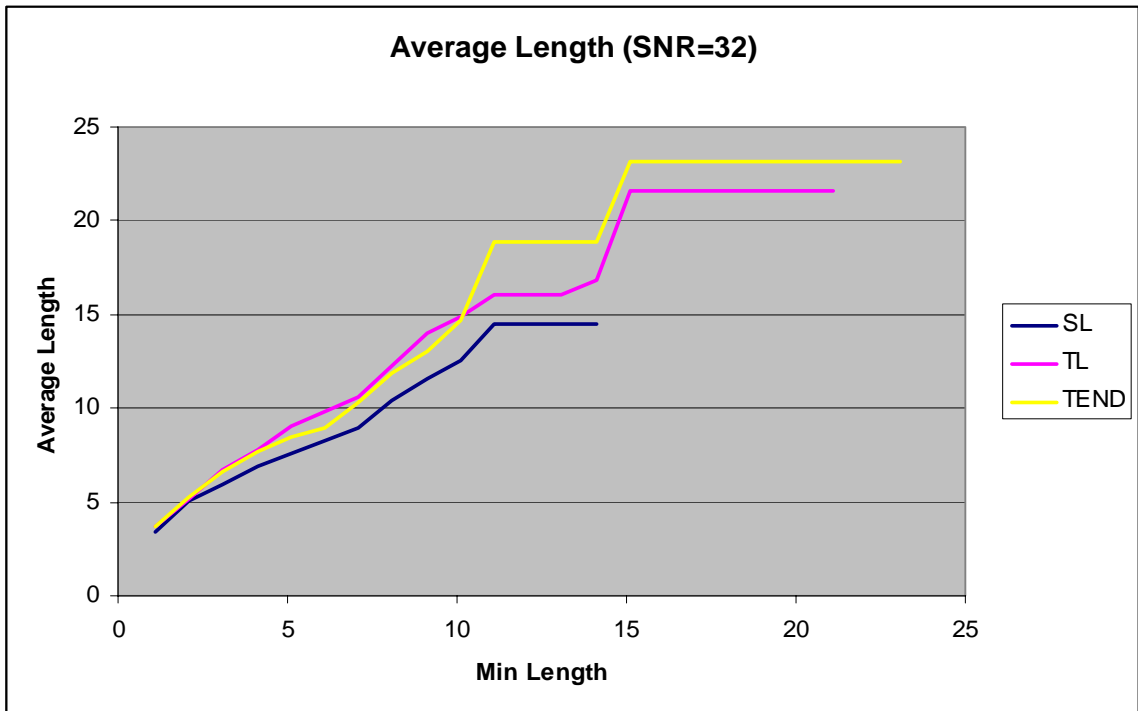
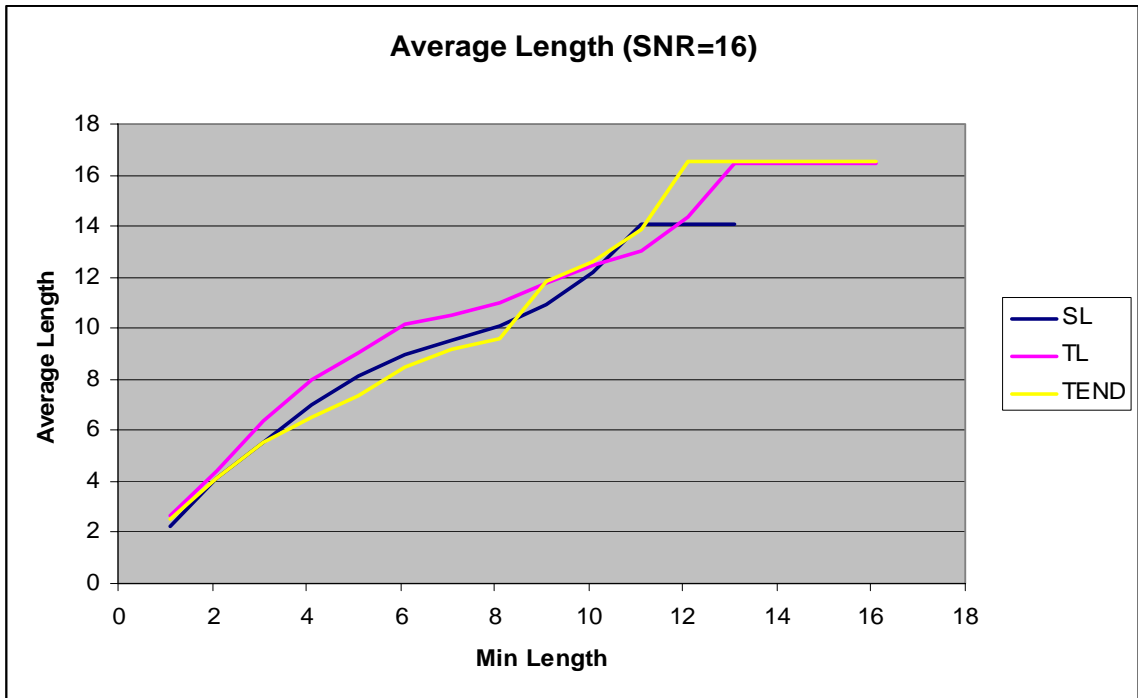
### Error Measurements of a Synthetic tensor field containing crossing tracts

The error measurements are done on the synthetic tensor field containing the crossing fiber tracts which are described in Section “Implementation” and depicted in Figure 8. First, we look at the changes of average length of the integrated tracts on the synthetic tensor field with different levels of SNR without considering the tracts’ correctness.

#### Error measurements of the average length of the simulated tracts

The average length is defined as a function of the minimum length which is the integration condition for the simulation of the tracts. The whole length of the ideal pathway in the synthetic tensor field is approximate 28 units.





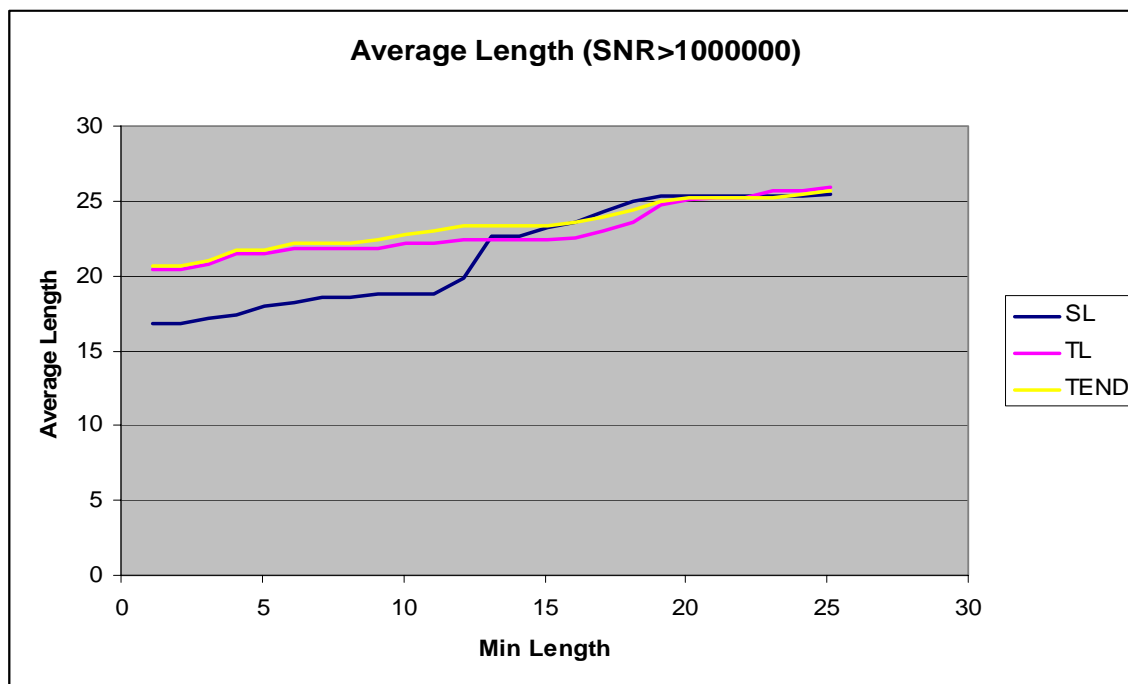


**Figure 13: The changes of Average length of estimated tracts with levels of SNR ( 8, 16, 32 and over 1000000).**

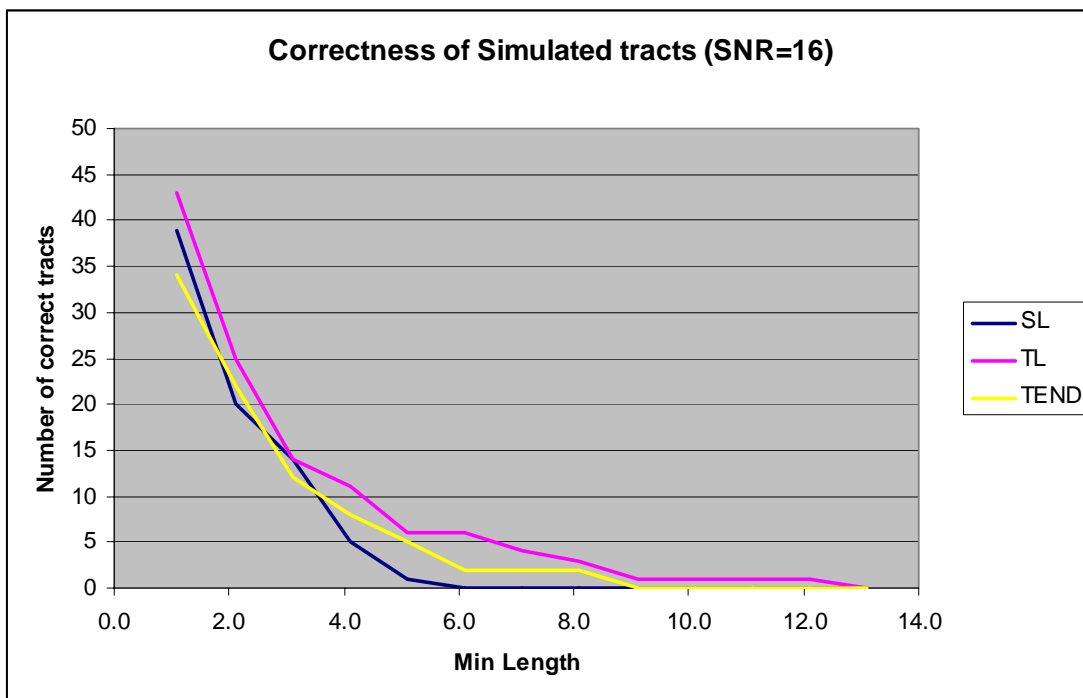
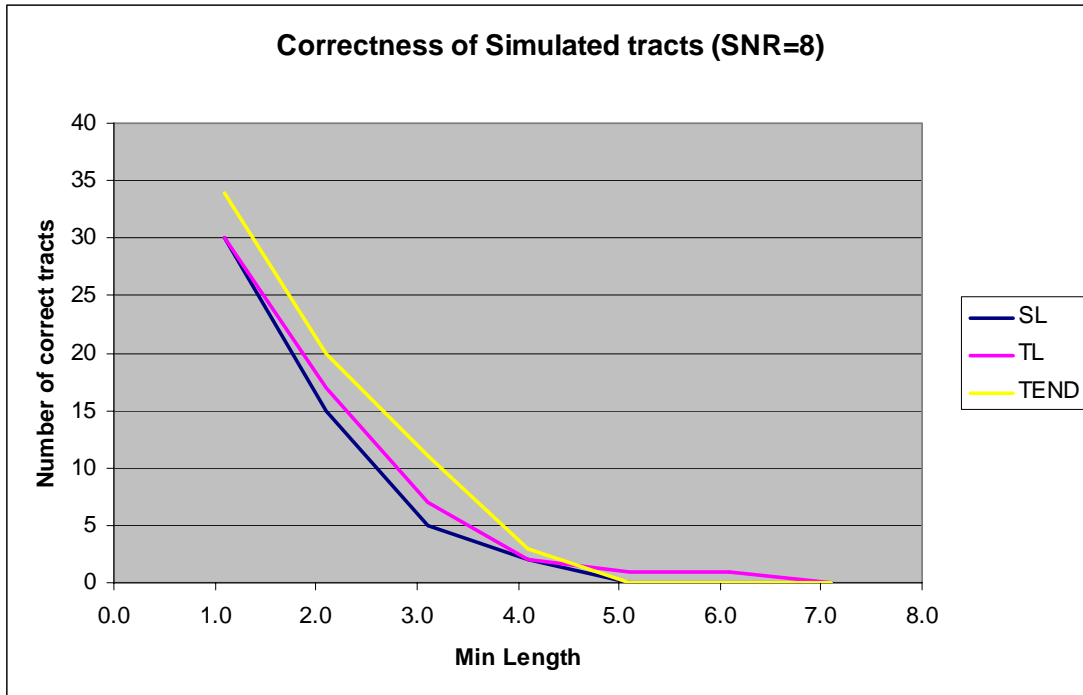
From the four charts rendered in Figure 13, it is obvious that TEND and Tensorline generate much longer tracts than Streamline in the tensor field with lower SNR. At same situation, TEND is better than Tensorlines in terms of propagating longer pathways.

When we study the white matter connectivity in vivo, the correctness of the tracts are most important than other aspects, such as length, smoothness of the tracts. If the simulated tracts can not represent the correct fiber tracts, it is pointless to study and analyze such estimated tracts. Hence, another error measurement which has been done in the application is measuring the number of correct tracts which follow the ideal pathways which are constructed by using B-Spline space curves.

### **Error measurements of the correctness of the simulated tracts**

A simulated tract is verified as correctly following the ideal pathway by testing both of its end points inside the B-Spline tube which represent the ideal pathway. Figure 14 includes 4 charts which demonstrate the changes of the number of the correct tracts along with the minimum length on the synthetic tensor fields with different levels of SNR. For example, the three methods can not propagate any

correct tracts when the minimum length that is the integration condition is increased more than 13 units when the tensor field with SNR of 16.



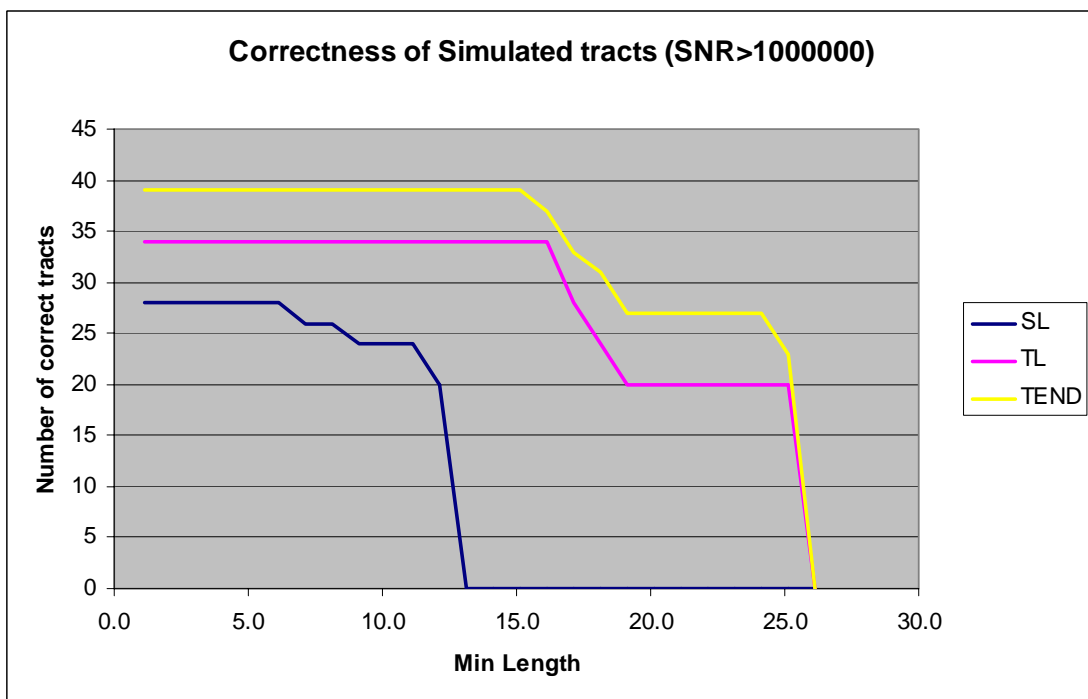
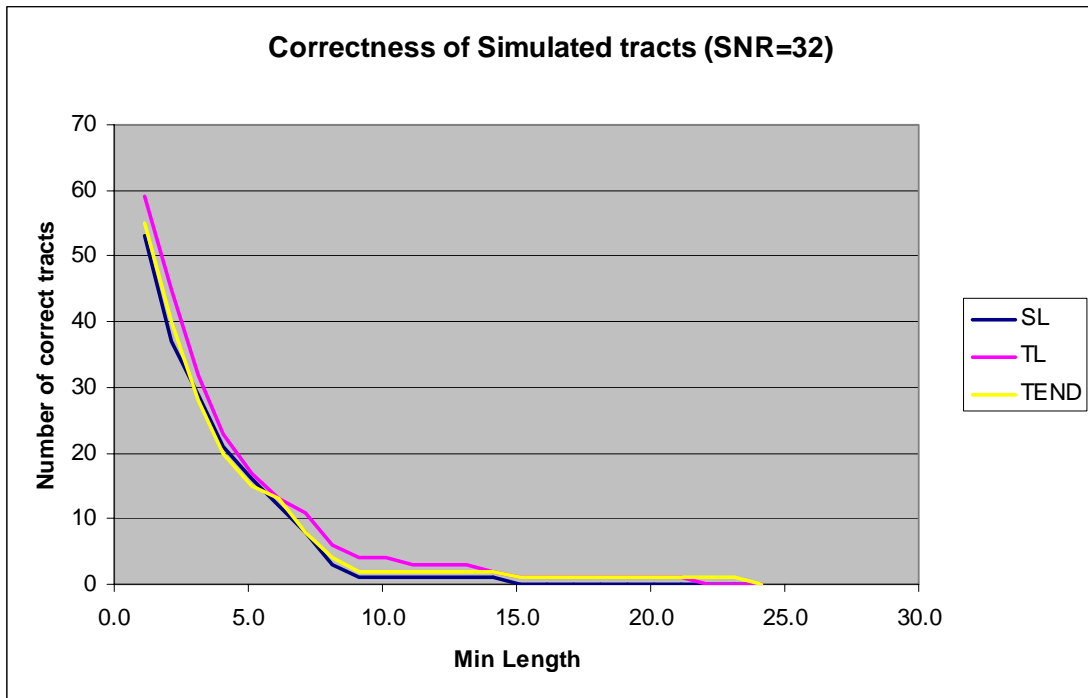


**Figure 14: Error measurement of correctness of tracts of a synthetic tensor field containing crossing fiber tracts.**

We can see the three methods do not make much difference in generating correct tracts when the synthetic tensor fields with lower SNR (such as 8, 16, and 32) from the first three charts. When the SNR increases to almost an infinite number, the synthetic tensor field is not affected by any noises, and the tensors are homogeneous

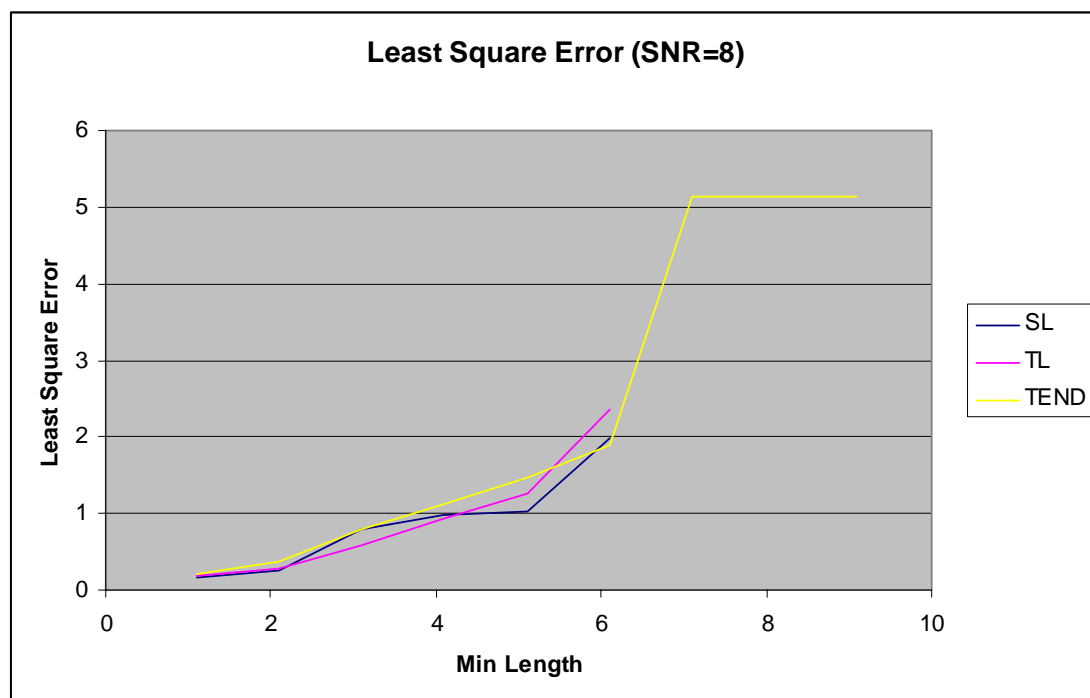
in all regions except the center where the two ideal pathways cross. In such situation, Streamlines method can not generate any correct tracts when minimum length is increased over half of the ideal pathway's length. Though Streamline still propagates longer and smooth tracts, all tracts deviate away from the right tracks when the simulation enters into the region containing complex connectivity, such as tract crossing, merging. On the other hand, Tensorlines and TEND methods do a much better job than Streamline in such complex regions. Moreover, from the last chart of Figure 14, TEND does a little bit better job than Tensorlines in terms of integrating correct tracts.

### Least Square Error of the simulated tracts

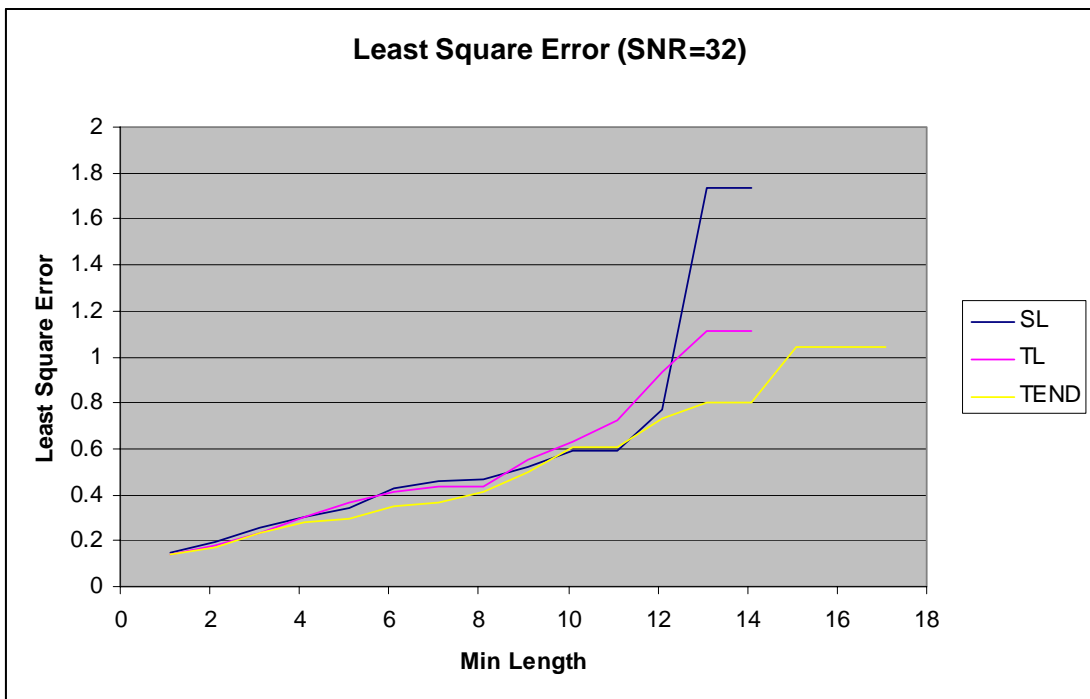
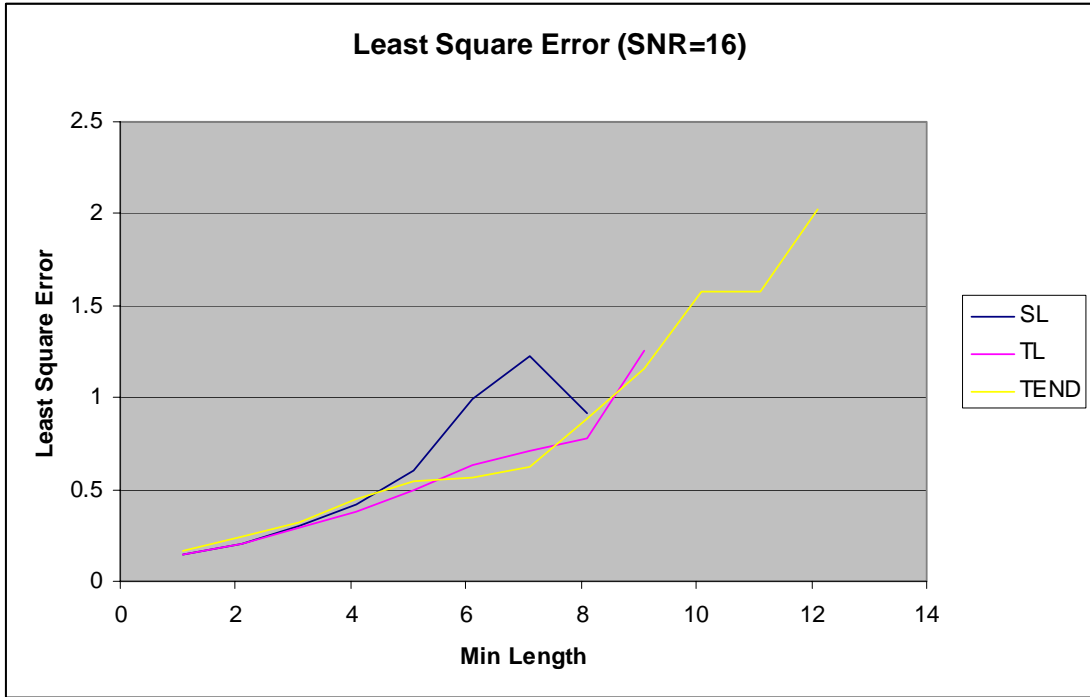
The least square error (LSE) is defined in Eq. [26].

$$LSE = \frac{\sqrt{\sum_{i=1}^n (\Delta\mathcal{E})^2}}{n} \quad \text{Equation 26}$$

where  $n$  is the number of the correctly simulated tracts which are following the ideal pathways;  $\Delta\mathcal{E}$  is the minimum distance from the each sample point on the simulated tracts to the ideal tracts, which is computed by finding the closest point on the B-Spline curve. The finding the closest point on the space curve is described in Implementation section.







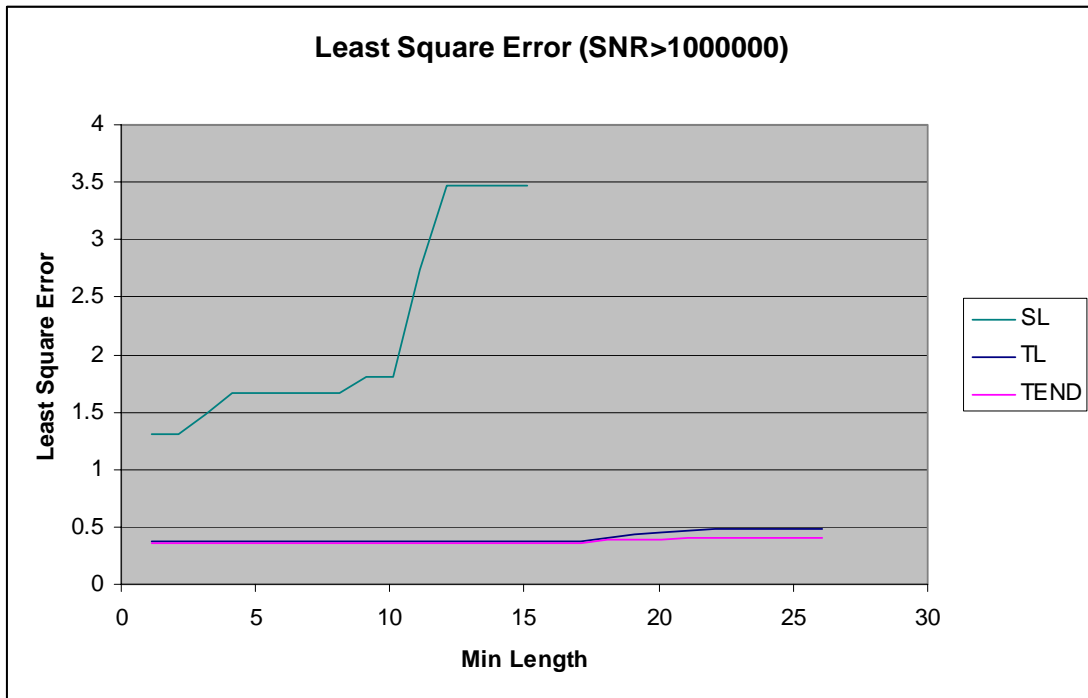


**Figure 15: The Least Square Error of the simulated tracts.**

The first three graphs in Figure 15 indicate that the three methods do not make much difference when the tensor fields with lower levels of SNR and the minimum length is set to a small number. The last graph shows that on the synthetic tensor field with higher levels of SNR that is great than 1000000, the simulated tracts generated by using Tensorlines and the Tensor deflection methods have much more lower LSE which keeps lower than 0.5, than the simulated tracts propagated by using Streamlines which have much more bigger LSE which is never lower than 1. The last graph also indicates that the TEND method does a little better job than the Tensorlines on such synthetic tensor fields. The result is similar as the error measurement results of the correctness of the tracts described in previous section.

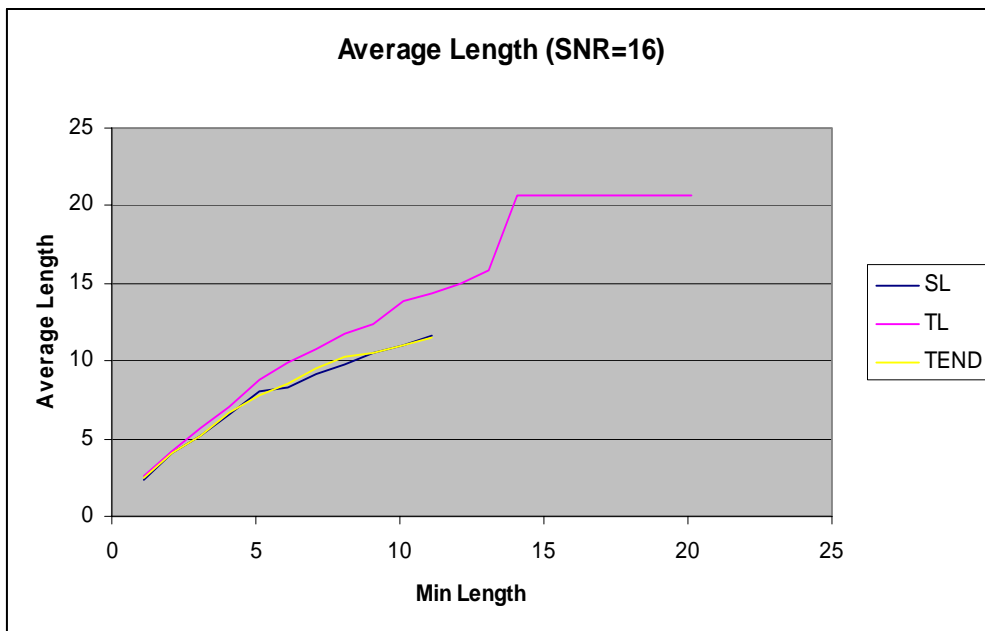
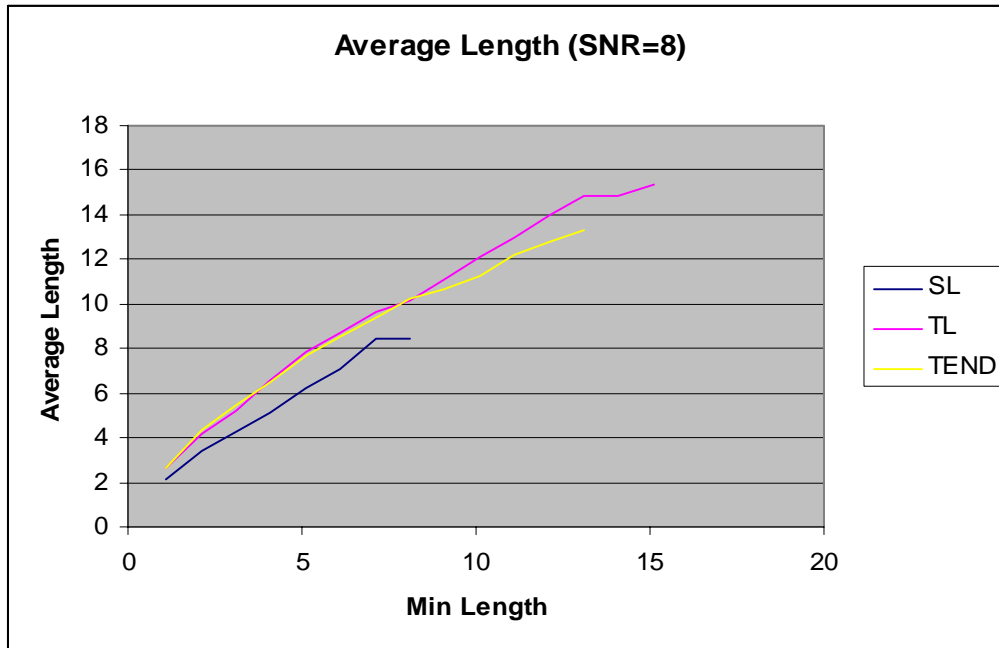
### **Error Measurements of a Synthetic tensor field containing merging tracts**

The error measurements are also done on the synthetic tensor fields containing the merging fiber tracts which are described in Section “Implementation” and depicted in Figure 9. Similarly as the error measurement done on the synthetic tensor fields containing crossing fiber tracts, first we exam the changes of average length of the integrated tracts on the synthetic tensor field with different levels of SNR without considering the tracts’ correctness, then test the correctness of the tracts, finally exam

the Least Square Error of the simulated tracts. The whole length of the ideal pathway in the field is about 29 units.

### Error measurements of the average length of the simulated tracts

The error measurements are presented in graphs.



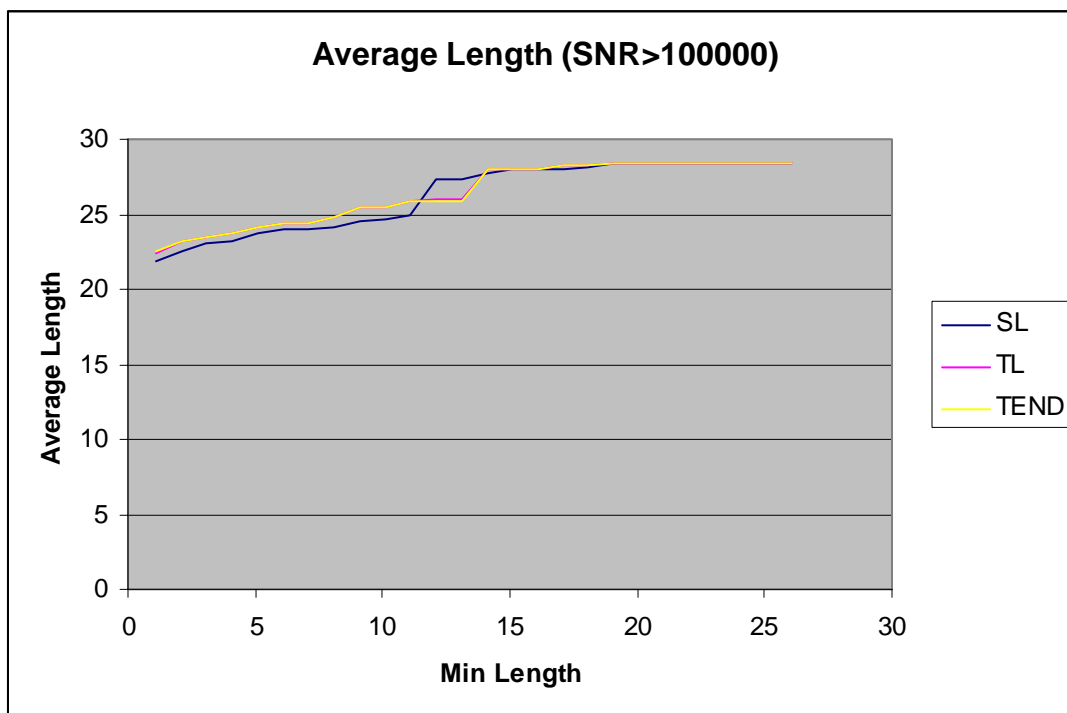
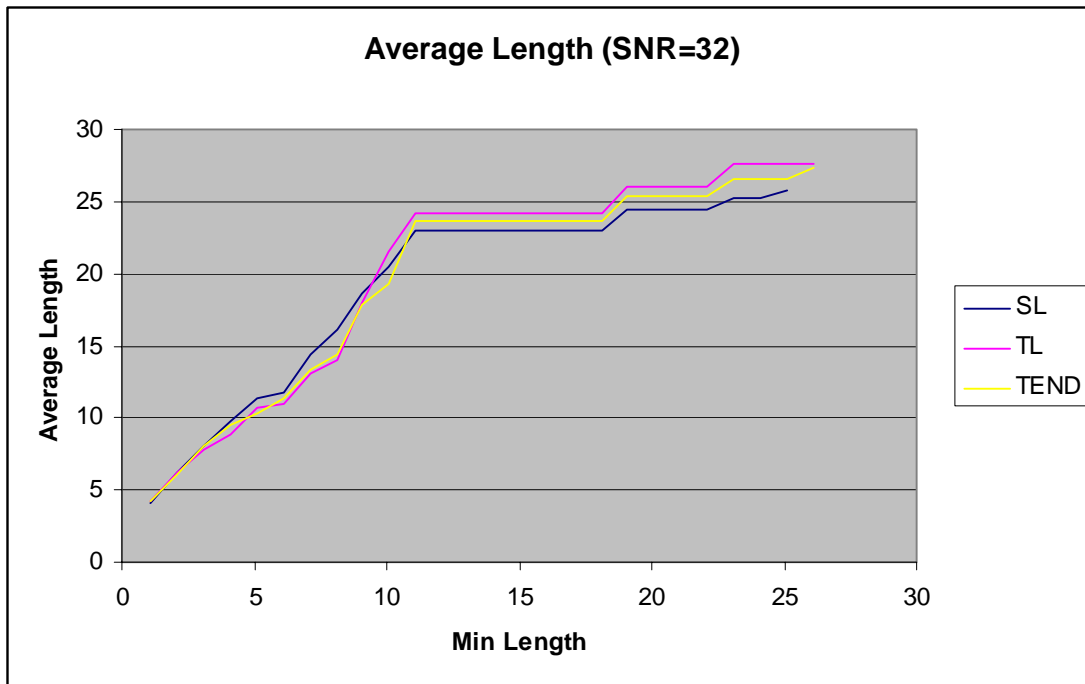


**Figure 16: The changes of Average length of estimated tracts with levels of SNR ( 8, 16, 32 and over 1000000).**

From the first two charts in Figure 15, The Tensorlines algorithm generates longer simulated tracts than Streamlines and TEND methods do when the tensor fields with lower levels of SNR. In order to see the difference among the Streamlines, Tensorlines and TEND methods in the last chart in the Figure 15, Table 1 shows the

dataset which is depicted in the last chart. From the last two charts and the Table 1, we can see that when the levels of SNR of the tensor fields become to 32 and over 32, the three methods have quiet similar results.

**Table 1: The average length over the min length (SNR>1000000)**

minLength	SL	TL	TEND	minLength	SL	TL	TEND
1.1	21.8241	22.4662	22.4921	14.1	27.7164	28.0264	28.0323
2.1	22.5336	23.1963	23.2232	15.1	27.9353	28.0264	28.0323
3.1	23.0103	23.4407	23.4679	16.1	27.9353	28.0264	28.0323
4.1	23.2411	23.674	23.7014	17.1	27.9353	28.2072	28.2132
5.1	23.7014	24.1454	24.1735	18.1	28.1023	28.2072	28.2132
6.1	23.9339	24.3732	24.4017	19.1	28.4495	28.3745	28.3793
7.1	23.9339	24.3732	24.4017	20.1	28.4495	28.3745	28.3793
8.1	24.1392	24.7963	24.8255	21.1	28.4495	28.3745	28.3793
9.1	24.5376	25.4404	25.4708	22.1	28.4495	28.3745	28.3793
10.1	24.7304	25.4404	25.4708	23.1	28.4495	28.3745	28.3793
11.1	24.9148	25.8418	25.873	24.1	28.4495	28.3745	28.3793
12.1	27.273	26.0375	25.873	25.1	28.4495	28.3745	28.3793
13.1	27.273	26.0375	25.873	26.1	28.4495	28.429	28.4339

### Error measurements of the correctness of the simulated tracts

Then three methods are tested in term of generating the correct tracts which are following the ideal pathways. The datasets obtained from the error measurement employed on the synthetic tensor fields with different levels of SNR are listed in Table 2 to Table 5 rather than graphs as it is hard to see the difference from graphs.

**Table 2: Number of the correct tracts over the min length (SNR=8)**

minLength	SL	TL	TEND	minLength	SL	TL	TEND
1.1	29	25	28	6.1	0	1	1
2.1	17	14	13	7.1	0	1	1
3.1	8	9	7	8.1	0	1	0
4.1	3	6	4	9.1	0	0	0
5.1	1	3	2				

**Table 3: Number of the correct tracts over the min length (SNR=16)**

minLength	SL	TL	TEND	minLength	SL	TL	TEND
1.1	37	36	35	7.1	2	2	3
2.1	24	25	23	8.1	1	1	1
3.1	13	15	12	9.1	1	1	1
4.1	9	11	9	10.1	1	1	1
5.1	3	5	4	11.1	0	0	0
6.1	3	5	4				

**Table 4: Number of the correct tracts over the min length (SNR=32)**

minLength	SL	TL	TEND	minLength	SL	TL	TEND
1.1	40	44	41	14.1	3	3	3
2.1	31	35	33	15.1	3	3	3
3.1	23	26	24	16.1	3	3	3
4.1	16	19	18	17.1	3	3	3
5.1	12	14	16	18.1	3	3	3
6.1	11	13	12	19.1	3	3	3
7.1	8	9	9	20.1	3	3	3
8.1	7	9	9	21.1	3	3	3
9.1	5	6	6	22.1	3	3	3
10.1	4	4	5	23.1	2	2	2
11.1	3	3	3	24.1	2	2	2
12.1	3	3	3	25.1	1	2	2
13.1	3	3	3	26.1	0	2	1

**Table 5: Number of the correct tracts over the min length (SNR>1000000)**

minLength	SL	TL	TEND	minLength	SL	TL	TEND
1.1	61	60	60	14.1	55	55	55
2.1	61	60	60	15.1	54	55	55
3.1	61	60	60	16.1	54	55	55
4.1	61	60	60	17.1	54	54	54
5.1	61	60	60	18.1	54	54	54
6.1	61	59	59	19.1	54	54	54
7.1	61	59	59	20.1	54	54	54
8.1	60	58	58	21.1	54	54	54
9.1	58	57	57	22.1	54	54	54
10.1	57	57	57	23.1	54	54	54
11.1	56	55	55	24.1	54	54	54
12.1	55	55	55	25.1	54	54	54
13.1	55	55	55	26.1	54	53	53

When SNR is lower and minimum length is smaller, Tensorlines and TEND methods do a little bit better job than Streamlines algorithm. However the results of the error measurement for the three methods are very similar when the value of the SNR of the synthetic tensor fields is higher than 1000000. This is different from the same error measurements done to the synthetic tensor fields with geometry of crossing tracts, which are described in previous section. This is because the synthetic tensor fields (Figure 9) containing merging tracts with high level of SNR almost are anisotropic in the regions containing the fiber tracts which merge together to be a single bundle of tracts, and the synthetic tensor fields (Figure 8) containing the crossing tracts with whatever level of SNR are not anisotropic in the region where two tracts cross each other.

## Least Square Error of the simulated tracts

The LSE is computed using Eq. 26 and the results of the error measurement are presented in tables rather than graphs as the differences of the three methods are not obvious to be seen in graphs.

**Table 6: Least Square Error (SNR=8)**

minLength	SL	TL	TEND	minLength	SL	TL	TEND
1.1	0.187352	0.228236	0.228929	5.1	1.15345	1.05002	1.26614
2.1	0.245145	0.339293	0.416951	6.1	Not valid	2.69748	2.30686
3.1	0.401325	0.476245	0.512679	7.1	Not valid	2.69748	2.30686
4.1	0.852262	0.635407	0.758163	8.1	Not valid	2.69748	Not valid

**Table 7: Least Square Error (SNR=16)**

minLength	SL	TL	TEND	minLength	SL	TL	TEND
1.1	0.150924	0.150036	0.153241	6.1	0.891907	0.607536	0.813095
2.1	0.207892	0.192014	0.207385	7.1	1.26167	1.13778	1.05
3.1	0.339747	0.285552	0.344629	8.1	0.510967	0.564326	0.519166
4.1	0.430911	0.348086	0.427186	9.1	0.510967	0.564326	0.519166
5.1	0.891907	0.607536	0.813095	10.1	0.510967	0.564326	0.519166

**Table 8: Least Square Error (SNR=32)**

minLength	SL	TL	TEND	minLength	SL	TL	TEND
1.1	0.167134	0.173625	0.181884	14.1	1.47771	1.58867	1.64694
2.1	0.207339	0.205514	0.218633	15.1	1.47771	1.58867	1.64694
3.1	0.26786	0.268389	0.290786	16.1	1.47771	1.58867	1.64694
4.1	0.356267	0.339106	0.356317	17.1	1.47771	1.58867	1.64694
5.1	0.44814	0.426445	0.381744	18.1	1.47771	1.58867	1.64694
6.1	0.488404	0.45886	0.506477	19.1	1.47771	1.58867	1.64694
7.1	0.629796	0.638573	0.654455	20.1	1.47771	1.58867	1.64694
8.1	0.695319	0.638573	0.654455	21.1	1.47771	1.58867	1.64694
9.1	0.966629	0.90241	0.955252	22.1	1.47771	1.58867	1.64694
10.1	1.20334	1.28251	1.14289	23.1	1.13969	1.14511	1.1202
11.1	1.47771	1.58867	1.64694	24.1	1.13969	1.14511	1.1202
12.1	1.47771	1.58867	1.64694	25.1	1.67759	1.14511	1.1202
13.1	1.47771	1.58867	1.64694	26.1	Not valid	1.14511	1.60319

**Table 9: Least Square Error (SNR>1000000)**

minLength	SL	TL	TEND	minLength	SL	TL	TEND
1.1	0.235111	0.234524	0.235674	14.1	0.213207	0.215855	0.217251
2.1	0.235111	0.234524	0.235674	15.1	0.207818	0.215855	0.217251
3.1	0.235111	0.234524	0.235674	16.1	0.207818	0.215855	0.217251
4.1	0.235111	0.234524	0.235674	17.1	0.207818	0.216664	0.218136
5.1	0.235111	0.234524	0.235674	18.1	0.207818	0.216664	0.218136
6.1	0.235111	0.232685	0.233861	19.1	0.207818	0.216664	0.218136
7.1	0.235111	0.232685	0.233861	20.1	0.207818	0.216664	0.218136
8.1	0.235114	0.232242	0.233497	21.1	0.207818	0.216664	0.218136
9.1	0.226538	0.226592	0.227823	22.1	0.207818	0.216664	0.218136
10.1	0.22454	0.226592	0.227823	23.1	0.207818	0.216664	0.218136
11.1	0.218967	0.215855	0.217251	24.1	0.207818	0.216664	0.218136
12.1	0.213207	0.215855	0.217251	25.1	0.207818	0.216664	0.218136
13.1	0.213207	0.215855	0.217251	26.1	0.207818	0.209722	0.211252

From the datasets listed in Table 6-9, we can see that the three methods have very similar results of the measurements of the Least Square Error. However, when the synthetic tensor fields which contain merging tracts have high levels of SNR, the simulated tracts generated by using Streamlines algorithm have smaller LSE than the tracts generated by using Tensorlines and TEND methods. The results of the measurement of LSE are similar as the results of the error measurement of the correctness of tracts for the synthetic tensor fields with the geometry of merging tracts.

The results of the three error measurements are in accordance with the purpose of the Tensorlines and Tensor Deflection methods, which are designed to deal with the un-anisotropic tensors. In a anisotropic tensor field, the three methods should generate similar tracts.



## CONCLUSIONS

A platform is created to test fiber tracking algorithms on noise-affected synthetic tensor fields. The platform is easy to be extended by adding new types of synthetic tensor fields or new fiber tractography methods for testing. Due to time constraints, we could stimulate and test only two fiber configurations. The error measurements in terms of average length of the estimated tracts, the number of correct tracts and the Least Square Error of tracts are analyzed on noise-contaminated synthetic fields containing crossing tracts and merging tracts with different levels of SNR respectively. The limit results of error measurements indicate Tensorlines and TEND are more suitable for inhomogeneous tensor fields than Streamline.

The three methods are not tested on linear or radiant homogeneous tensor fields in this project as Lazar and Alexander have done it in 2003(Lazar and Alexander 2003). More testing has to be done to obtain a better understanding of the advantage and disadvantage of the three fiber tracking methods. And also, more fiber tractography methods should be tested, such as Markov chain algorithm.

When adding noises to the synthetic tensor in the project, the B-factor is assumed to  $b = 1000 \frac{s}{mm^2}$  simply. The value may not be suitable for inhomogeneous tensors containing more complex fiber connectivity. The effect of choosing of B-factor should be considered when constructing synthetic tensor fields for testing fiber tractography methods.

## ACKNOWLEDGEMENTS

Many thanks to Burkhard for his supervision on the project. I greatly appreciated the help from Lisa Jonasson, Donald Tournier and Peter Basser who answered my questions promptly and clearly and sent me the papers that I could not find on the internet. Without their help, I doubt I could finish the work.

## REFERENCES

- Basser, P. J., S. Pajevic, et al. (2000). "In vivo fiber tractography using DT-MRI data." Magnetic Resonance in Medicine **44**(4): 625-632.
- Gubjartsson, H. and S. Patz (1995). "The Rician distribution of noisy MRI data." Magn Reson Med **34**: 910-914.
- Henkelman, R. (1985). "Measurement of signal intensity in the presence of noise in MR images." Med Phys **12**: 232-233.
- Hesselink, L., Y. Levy, et al. (1997). "The topology of symmetric, second-order 3D tensor fields." IEEE Transactions on Visualization and Computer Graphics **3**(1): 1-11.
- Jonasson, L., X. Bresson, et al. (2005). "White matter fiber tract segmentation in DT-MRI using geometric flows." Medical Image Analysis **9**(3): 223-236.
- Jonasson, L., P. Hagmann, et al. (2003). White Matter Mapping in DT-MRI using geometric flows. 9th International Conference on Computer Aided Systems Theory, Las Palmas de Gran Canaria, Spain.
- Lazar, M. and A. L. Alexander (2003). "An error analysis of white matter tractography methods: synthetic diffusion tensor field simulations." Neuroimage **20**: 1140-1153.
- Lazar, M., D. M. Weinstein, et al. (2003). "White matter tractography using diffusion tensor deflection." Human Brain Mapping **18**(4): 306-321.
- Mori, S. and P. C. M. v. Zijl (2002). Fiber tracking: principles and strategies - a technical review. NMR in Biomedicine. **15**: 468-480.
- Papadakis, N. G., D. Xing, et al. (1999). "A Comparative Study of Acquisition Schemes for Diffusion Tensor Imaging Using MRI." Journal of Magnetic Resonance **137**: 67-82.
- Pierpaoli, C., P. Jezzard, et al. (1996). "Diffusion tensor MR imaging of the human brain." Radiology **201**(3): 637-648.

Press, W. H., B. P. Flannery, et al. (1992). Numerical Recipes in C: The Art of Scientific Computing. Cambridge, Cambridge University Press.

Shahar, A. R. B. "The Human Brain." <http://www.imt.co.il/humanbrain.htm>.

Skare, S., T.-Q. Li, et al. (2000). "Noise considerations in the determination of diffusion tensor anisotropy." Magnetic Resonance Imaging **18**(6): 659-669.

Tuch, D. S. (2004). "Q-Ball Imaging." Magnetic Resonance in Medicine **52**: 1358-1372.

Weinstein, D. M., G. Kindlmann, et al. (1999). Tensorlines: Advection-diffusion based propagation through diffusion tensor fields. Proceedings of Visualization.

Westin, C.-F., S. E. Maier, et al. (1999). Image processing for diffusion tensor magnetic resonance imaging. Medical Image Computing and Computer-Assisted Intervention, Cambridge, UK, Springer Verlag.

Westin, C.-F., S. Peled, et al. (1997). Geometrical diffusion measures for MRI from tensor basis analysis. Proceeding of ISMRM.

Wuenschel, B. (2004). Visualization Techniques for Vector Fields. Computer Science 716 lecture notes, The university of auckland (<http://www.cs.auckland.ac.nz/compsci716s2t/lectures/>).

Wuenschel, B. and R. Lobb (2003). The 3D visualization of brain anatomy from diffusion-weighted magnetic resonance imaging data. Computer graphics and interactive techniques in Australasia and South East Asia.

Young, E. C. (1993). Vector and Tensor Analysis, Marcel Dekker, Inc.